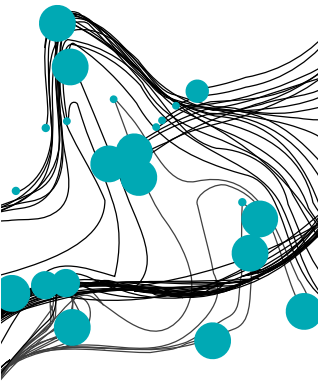

RAM ROBOTICS AND MECHATRONICS

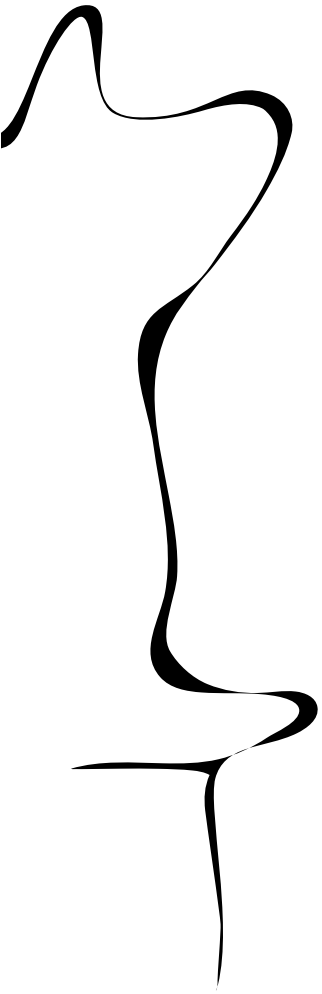

Evaluation of the SUNRAM 5 for performing a full clinical in-situ breast biopsy procedure

G.S. (Gaurav) Bhide

MSC ASSIGNMENT

Committee:
prof. dr. ir. L. Abelmann
dr. V. Groenhuis
dr. F.S. Siepel
prof. dr. ir. R.M. Verdaasdonk

August 2020

044RaM2020
Robotics and Mechatronics
EEMCS
University of Twente
P.O. Box 217
7500 AE Enschede
The Netherlands

UNIVERSITY OF TWENTE. | TECHMED CENTRE
UNIVERSITY OF TWENTE. | DIGITAL SOCIETY INSTITUTE

Abstract

Breast cancer, one of the most dangerous diseases, poses a significant risk to the patient if left untreated. One of the methods for breast cancer screening and diagnosis is MRI guided breast biopsy. Since manual systems lack in accuracy and efficiency, and the procedure time required for MRI based biopsy is very high, a set of robotic systems were developed to perform MR safe robot-assisted biopsy. The current SUNRAM 5 robot, the 5th robot of the series, is a 5 DOF system including a breast fixation system, an emergency needle ejection mechanism, and fast and precise needle insertion under near real-time MRI guidance. The robot has been programmed to operate to target green dye stained PVC plastisol blocks (mimicking lesions) in breast phantoms inside a 0.25T MRI scanner. Evaluation of the system was performed in air and based on the MRI scan. Additionally, a full clinical biopsy procedure workflow was developed using the SUNRAM 5 and an easy to operate user interface. The robot achieved submillimeter accuracy and precision in targeting the targets in air. MRI based evaluation was considered successful with an average maximum error of 1.24mm in the X direction and 3.52mm in the Y direction. A full clinical biopsy workflow was tested in using a simple-to-use app and the average procedure time excluding the time taken for taking the MRI scans was recorded to be around 3 mins and 25 seconds.

Contents

List of Figures

List of Tables

1 Introduction

The global burden of cancer continues to increase largely because of aging and an increase in population as well as the adoption of cancer-causing behaviors. Breast cancer is the most frequently diagnosed cancer and the leading cause of cancer deaths in females (Jemal et al. (2011)). As GLOBOCAN reports, in the year 2018, there have been around 2 million new breast cancer cases in the world and the mortality rate for breast cancer is around 7 % [Source - Global Cancer Observatory(https://gco.iarc.fr/)]. Early diagnosis of breast cancer is necessary for treatment and extensive screening programs are available in many countries. During the diagnosis phase, imaging techniques can be used to detect one or more suspicious lesions (abnormalities) found in the breast. At this stage, it is necessary to perform a biopsy to extract a tissue sample from the lesion for further examination. The biopsy procedure involves inserting a hollow needle towards the lesion followed by a firing sequence in which a sample of the lesion is cut off and later extracted for further investigation. In cases where the lesion is not visible on X-Ray or ultrasound, MRI guided biopsy is the method used for correctly identifying suspicious lesions and extracting them.

Since the accuracy of manual biopsy based on MRI scan is comparatively low and the procedure time is extremely high owing to the need of acquiring multiple MRI scans as well as getting the patient in and out of the MRI many times, a set of robotic systems were developed, at the University of Twente, to perform MR safe robot-assisted biopsy. The systems, developed by the RaM (Robotics and Mechatronics) group at the University of Twente, are currently in the 5th generation of development and the current robot, the SUNRAM 5, is a 5DOF robot driven by six linear and curved pneumatic stepper motors & three cylinders all constructed using rapid prototyping. The SUNRAM 5 robot includes a breast fixation system, an emergency needle ejection mechanism, and fast and precise needle insertions under near real-time MRI guidance, thus capable of performing a full clinical in-situ breast biopsy procedure.

1.1 Problem Statement Analysis

As compared to the earlier editions of the robot, which will be put forward in the upcoming section, the SUNRAM 5 has a new kinematic design along with a unique breast fixation system. This fixation system allows the procedure to be completed with the patient (in our case the breast phantom) lying in the prone position. It is inspired by the breast fixation system developed by Machnet BV (Roden, The Netherlands). The breast fixation system has a grating with 5 pillars in the front with markers embedded inside the vertical coloumns. These markers are visible inside the MRI and are useful in localizing the position of the robot. The breast fixation system has been designed in order to minimize the movement of the breast and thereby reducing the inaccuracies due to needle tissue interactions. Additionally, the SUNRAM 5 also has a biopsy gun firing mechanism along with an emergency needle ejection system. Therefore, the robot is ideally suited for completing a full clinical in-situ breast biopsy procedure. Thirdly, another major upgrade in the SUNRAM 5 is the use of the dual-speed stepper motors. These motors have two different racks using which they can move at different speeds simultaneously. Therefore, all these factors have the potential to improve the accuracy and operating time of the robot. With the implementation of the biopsy gun firing mechanism, the robot now also has the potential to complete a full clinical breast biopsy procedure.

The aim of this study is to develop a full clinical breast biopsy procedure and evaluate the SUNRAM 5 in terms of space requirements, targeting accuracy, and operation time. In order to evaluate the robot, there are 2 important things that need to be established initially i.e.

the localization of the robot in the MRI environment using the pre-operative MRI scan and kinematic design and control of the robot to avoid the frame constraints. Another important part of this research is the performance evaluation of the dual-speed stepper motors and their effect on positioning accuracy and operating speed. After the implementation of the above-mentioned tasks, the SUNRAM 5 will be evaluated for its performance in air as well as in an MRI environment during a full clinical procedure. Eventually, this leads us to form our research question.

- How does the SUNRAM 5 with the Machnet inspired breast fixation system evaluate with respect to its predecessor, the Stormram 4?

Additionally, two sub research questions could also be formulated, the answers to which conclude the additional subtasks involved in evaluating the robot.

- How do the dual-speed stepper motors improve the performance of the robot in terms of the positioning accuracy and operating time?
- How does the SUNRAM provide the possibility to complete a full clinical in-situ breast biopsy procedure?

1.2 Hypothesis

Here, the hypothesis is that the SUNRAM 5 with its full operating capabilities will be an improvement in performance in terms of targeting accuracy and operating time. The robot will also possess the ability to complete a full clinical breast biopsy procedure inside the MRI scanner.

1.3 Sketch of the Proposed Solution

The robot is placed inside the MRI scanner along with the breast phantom fixed using the unique breast fixation system in the prone position. The controller for the pneumatic valves as well as the valves themselves have been placed outside the Faraday cage of the MRI scanner. The entire system will be integrated using a GUI in order to simplify the operation. Scans are made through the MRI and lesion is localized. Doctors can select the lesion manually with a mouseclick to drop a fiducial marker and pinpoint the target coordinates. The software translates the target coordinates in terms of the robot coordinate system and calculates the number of steps needed for the robot to reach the desired target location. The operator will then manually operate the robot in order to reach the desired positions. Another MRI scan will be made to localize the inserted needle position. A biopsy can then be performed. Factors such as physical bending of components causing them to deviate could have an effect on the accuracy of the robot eventually giving rise to discretization errors. The operator can finish the procedure by dragging back the controls to the base position thus bringing the robot back to its base position.

1.4 Experiments and Evaluation

Experiments will be defined for evaluation of the dual-speed stepper motors and for evaluating the targeting accuracy of the robot in air and inside the MRI scanner. The evaluation in air involves creating a grid of crosshairs aligned on a piece of paper and selecting them as targets for the robot. Once the test is completed for the accuracy in air, further the test will be extended to MRI evaluation. A phantom with green-dyed PVC Plastisol lesions is used for this purpose. The evaluation will be done using the unique breast fixation system inside the bore of the MRI scanner. A full MRI-guided biopsy workflow will be defined and the operation time of the robot will be evaluated. The entire evaluation procedure has been described further in detail along with the results and detailed recommendations have been put forth for future tasks.

2 Literature Survey

Survey for the existing literature was undertaken in the areas of imaging techniques, biopsy and MRI guided biopsy techniques, current literature in the areas of MRI safe robotics and breast fixation systems, research about prior development in areas of Stormram robotic systems and similar work undertaken in areas of automatic operating robots. Since the core aim of this research is to work on an MR safe robotic system for breast biopsy, the focus of the existing literature survey has been confined to breast biopsy and related material only. However, to have an idea about the overall developments in MRI robotics, a small part of the research has been dedicated to systems developed for MRI based applications not related to breast biopsy.

2.1 Imaging Techniques

Various two and three-dimensional techniques are available for analyzing the breast in order to find a suspicious lesion. Palpation, a non-imaging based technique, involves analyzing the breast through one's hands and is usually a very primitive method of diagnosis. It is only useful in cases where the lesion is big enough to be felt by hand and therefore it is not effective in cases of routine diagnostic checkups since the lesion could still be small and could be missed. Therefore, for detailed analysis, imaging technology is necessary. Every technique has its own advantages and disadvantages and a small overview of each technique has been put forward here.

2.1.1 Mammography

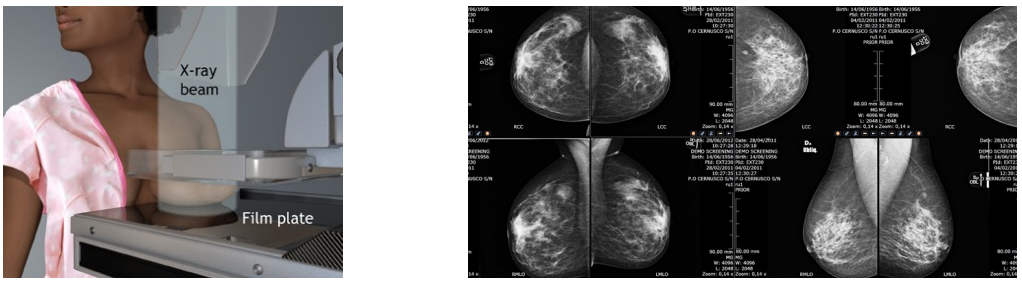

Figure 2.1: Left - Mammography Procedure, Source - [medlineplus.gov]
Right - Mammogram, Source - [esaote.com]

Mammography is a basic breast imaging technique which makes use of X-Rays to obtain two-dimensional black and white images. The breast is compressed between two plates and a small dose of radiation is used to obtain the X-Ray image. Various intricacies in the breast are visible, better if the breast is not too dense, and it is a useful technique for quick and basic diagnosis. Since this technique only gives a 2D image, it is difficult to distinguish between structures that are perpendicular to the image plane. If suspicious lesions are found, further detailed analysis could be done using an ultrasound.

2.1.2 Ultrasound

Figure 2.2: Left - Ultrasound Procedure, Source - [phillips.com]
Right - Breast Ultrasound with Lesion, Source - [densebreast-info.org]

Ultrasound technique makes use of very high frequency (several megahertz) acoustic waves to make an image of the breast in one plane. The waves are transmitted using a handheld device and these waves get attenuated and reflected off of tissue layers. These reflected waves are picked up again by the handheld device and an image is reconstructed based on the difference between the transmitted and reflected waves. Since the image is obtained with the handheld device, the image plane can be chosen almost arbitrarily. This has an advantage over mammography since a suspicious lesion can then be imaged, inspected, and analyzed from different angles. Also, another advantage is that ultrasound does not use ionizing radiation. The disadvantage of this procedure is that the imaging depth using ultrasound is usually only up to a few cms and there is a possibility that not all lesions are visible on ultrasound.

2.1.3 MRI

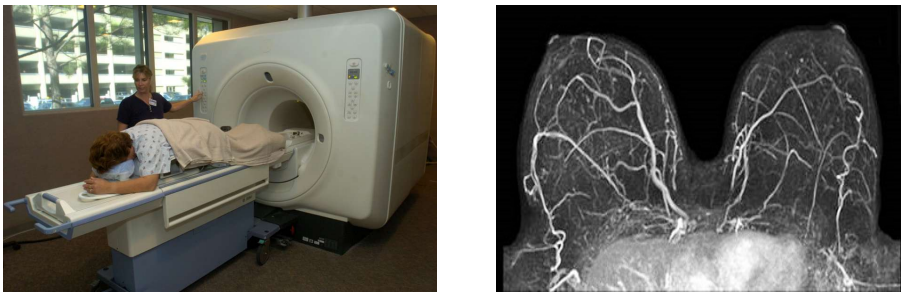

Figure 2.3: Left - Breast MRI Procedure, Source - [mrt.com]
Right - Breast MRI Scan, Source - [mdlinx.com]

Some lesions are not visible on mammography and ultrasound. MRI which stands for magnetic resonance imaging is a technique that has the highest sensitivity among other techniques and the best part is that it does not even generate ionizing radiations. However, MRI is also the most expensive technique among others. The MRI works based on resonance where the MRI scanner has a strong magnetic field with oscillating gradients which resonate with protons. With the introduction of a strong magnetic field, the protons tend to align themselves with the magnetic field. The introduction of a radiofrequency pulse can force the proton to misalign. Once the pulse is turned off, the protons will try to realign themselves and in-process generate a radio frequency wave. MRI scan has very high sensitivity compared to other techniques and thus it is almost always possible to identify a suspicious lesion if any from the MRI scan.

2.1.4 Elastrography, CT, PET, SPECT

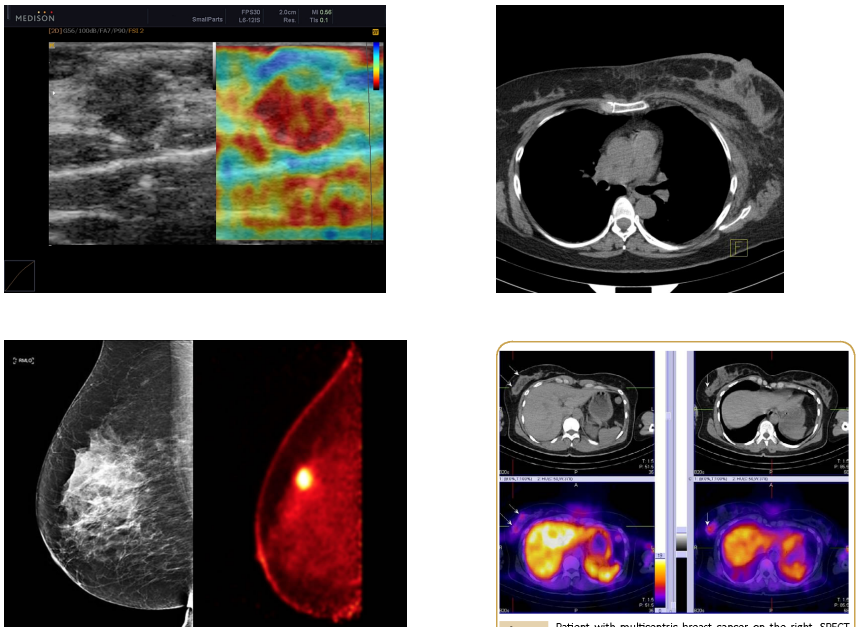

Figure 2.4: Left Top - Elastography, Source - [medison.com], Right Top - CT Scan, Source - [radiopaedia.org]
Left Bottom - PET Scan, Source - [breast360.org], Right Bottom - SPECT Scan, Source - [Sergieva (2015)]

Since the lesions usually have higher stiffness as compared to normal tissue, elastography techniques can also be used to image the breast. Strain imaging uses an external object pressed with known pressure against the breast introducing displacement and local deformation. The magnitude of these deformations can be measured using ultrasound. Then the ratio between stress and strain can give us the elasticity. MRI based procedure is also possible where shear waves are generated externally after which the velocity of these waves is measure using an MRI scanning sequence.

CT or the computed tomography technique uses X-ray imaging to take multiple X-Rays of the breast from various angles in order to be able to reconstruct a 3D image of the breast. PET or positron emission tomography and SPECT or single-photon emission CT also reconstruct breast images by detecting gamma rays emitted by radioactive tracers and visualizing the stream of fluids in the body. CT, PET, and SPECT all involve the use of ionizing radiation.

2.2 Breast Biopsy

The detection of a suspicious lesion is normally followed by a procedure to extract a tissue sample from the lesion for laboratory tests and this process is called as biopsy in our case breast biopsy. The biopsy procedure involves inserting a hollow needle into the breast at the right position followed by a firing sequence that cuts of a small sample of the lesion and extracts it. These samples are then clinically tested for malignancy which is followed up by the doctor's advice. Biopsy is a critical procedure and it is absolutely essential that the lesion must not be missed to avoid the possibility of a false negative biopsy.

2.2.1 Ultrasound-Guided breast biopsy

Figure 2.5: Patient undergoing Ultrasound-guided breast biopsy, Source - [radiologyinfo.org]

The manual ultrasound handheld probe scans the breast for the lesion and simultaneously the needle is inserted in the breast to get a tissue sample. The needle is manipulated by hand, by using the real-time feedback from the ultrasound, to reach its target. A sample is taken from the site and the biopsy procedure is complete. However, in this procedure, the drawback is that there might be some lesions that are still invisible on ultrasound and therefore not possible to be biopsied using ultrasound.

2.2.2 MRI Guided breast biopsy

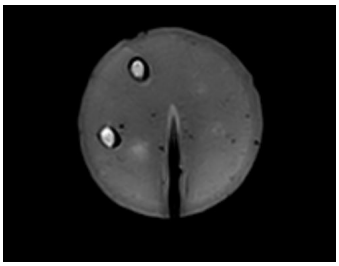

Figure 2.6: Left - MRI guided Breast Biopsy, Source - [healthmanagement.org]
Right - Breast MRI with Biopsy needle (Stormram 4)

In cases where the lesion is not visible on ultrasound, an MRI guided biopsy may be necessary.
A standard MRI guided breast biopsy procedure (https://www.med.unc.edu/radiology/breastimaging/services/mri-of-the-breast/mri-guided-breast-biopsy/) is as follows -

- Initially, the patient is made to lie down in a prone position on a biopsy table with the breast positioned into an opening on the table. The breast is then compressed between plates one of which has a grid structure.
- The patient is then given an intravenous drip and a contrast material intravenously for better visibility under MRI.
- The patient is then taken to an MRI scanner with all attachments removed. A pre-procedure MRI scan is performed (with and without the contrast agent) to locate the position of the lesion.
- Once the pre-procedural MRI scan is complete, the patient is brought out of the MRI scanner. A computer software is used to mark the location of the lesion with respect to the grid and the insertion depth.

- After the location is confirmed, a stylet through a sheath is inserted to create access to the lesion location. The stylet is then replaced by an obturator and the patient is again taken to the MRI room and scanned to confirm the location of the tip with respect to the lesion. If not, the last steps are repeated until the tip is at the right location.
- Once the location is confirmed, the patient is again brought out of the MRI scanner and a biopsy needle is inserted. Multiple samples are usually taken at the same time.
- Once the samples are taken, a localization clip is inserted and a confirmatory scan is taken to confirm the clip location either using an MRI or a Mammogram.

Therefore, there are still a few fundamental limitations with the current manual MRI guided biopsy procedure. The current procedure requires the patient to be taken in and out of the MRI scanner multiple times. Although the breast is fixed, it may move due to breathing, involuntary muscle actions, and needle tissue interaction. The grid system can also cause an error due to its resolution. The entire procedure takes about 60 minutes. The time taken is based on a lot of factors such as the strength of the MRI scanner (in standard hospital environments, scanners with strength 1.5T or 3T are used), skill of the operator, and ease of access to the biopsy site based on lesion size. Majority of the time is taken up by the MRI scanner itself (sometimes even 5-10 scans are required to be combined to locate the accurate lesion location) as well as the time taken to get the patient in and out of the MRI room. Also, a relatively thick needle (4mm) is inserted causing significant tissue damage. Due to such fundamental limitations, a more accurate and efficient system to perform MRI guided biopsies is needed which forms the basis of this research.

2.3 MRI based Robotic Systems - State of the Art

Increasing incorporation of robotics in the field of MRI safe operation is not a new challenge and a lot of research has already been done on the same. There have been multiple manual and automatic systems that have been developed which achieve their objective in a better way than the current clinical procedure. Multiple MR safe and MR conditional systems have been developed which specifically target various organs such as prostate area, liver, brain, breast, etc.

2.3.1 Brain

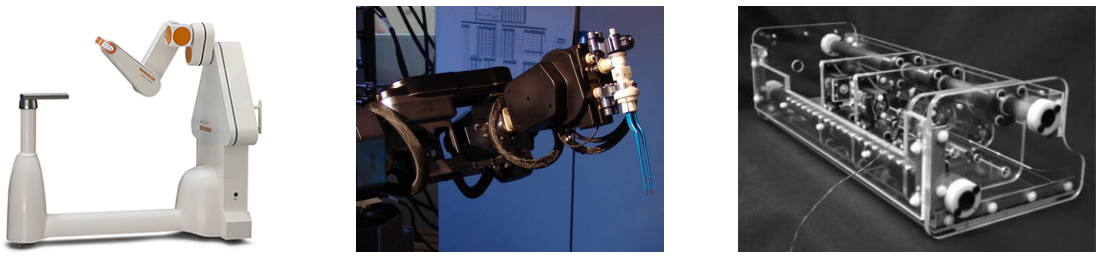

Figure 2.7: Left - NeuroMate Robot, Reinshaw Inc., Source - [reinshaw.com]
Center - Neuroarm, Source - [medgadget.com]
Right - Comber et al. (2012)

Brain operations are critical and medical procedures related to the brain include drug delivery, laser surgery, electrode placement for brain stimulation, and biopsy. Out of these, the NeuroMate Robot by Reinshaw Inc. is a robotic system that has been tested for DBS electrode placement using pre-operative MRI. However, only 37 of 50 attempts were successful with an accuracy of 1.7mm (Varma et al. (2003)). Masamune et al. also developed a surgical robot with

automatic registration capability. In addition to that, it also had an interactive MRI guided visualization of the brain. Both these functionalities help in improving the positioning, accuracy, repeatability, and safety (Masamune et al. (1998)). Lang et al. also developed a system called Neuroarm operated using piezoelectric motors for MR guided microsurgery. During the clinical trials, Neuroarm was also used in the routine dissection of the tumor brain interface (Lang et al. (2011)). Comber et al. also presented a pneumatically actuated robot for MRI guided neurosurgery. However, the presence of a large number of tubes resulted in non-linearity and difficulty in controlling the robot (Comber et al. (2012)). Another intraoperative MRI guided robot for bilateral stereotactic neurosurgery was developed by Guo et al. The robot had a compact design and capabilities to operate inside the imaging head coil. The robot was hydraulically actuated and achieved sufficient targeting accuracy (≤1.73mm). The robot also offered a real-time wireless tracking technique to localize the robot under MRI environment. Tests were performed to measure the robot localization as well as interference in the MRI image quality (Guo et al. (2018)).

2.3.2 Liver

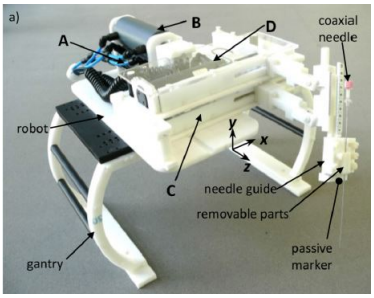

Figure 2.8: Franco et al. (2016)

A few systems exist which make use of MR safe/conditional robots for operating on the liver. Franco et al. developed a robotic system for use in laser ablation of liver tumors under the guidance of magnetic resonance imaging. The robot is capable of providing alignment of a needle guide inside the bore of the MRI scanner. The robot is controlled through pneumatic lines connected to control valves which are placed outside the Faraday cage of the MRI scanner. High position accuracy was achieved using a new time-delay scheme and a marker localization method was implemented to localize the robot in the MRI coordinates. This robotic system underwent two clinical studies with promising outcomes (Franco et al. (2016)).

2.3.3 Prostate

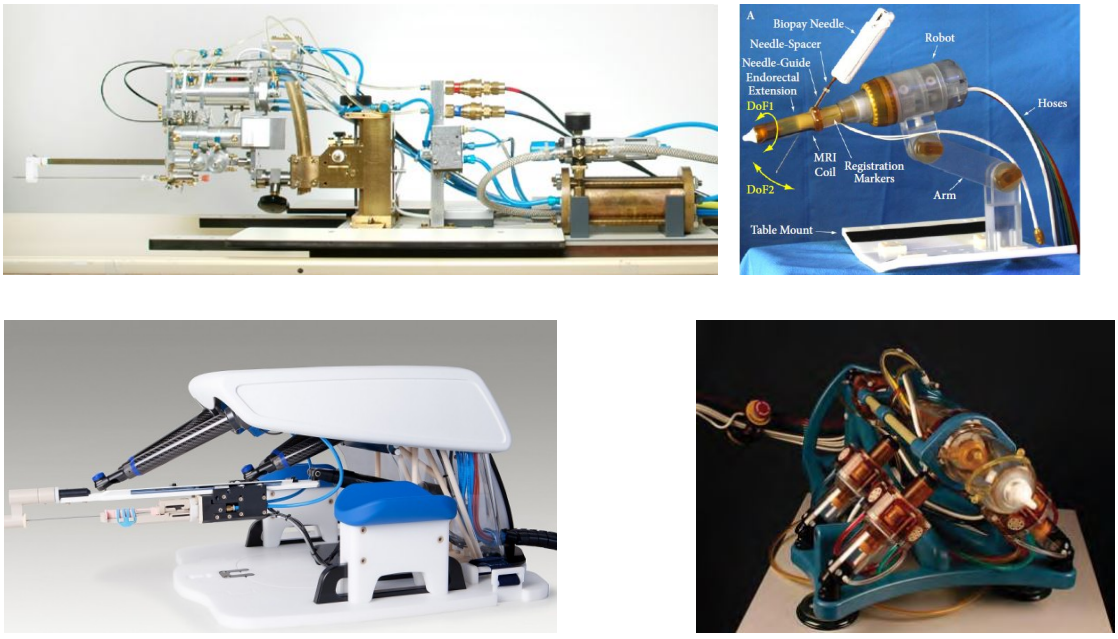

Figure 2.9: Left Top - Van den Bosch et al. (2010), Right Top - Stoianovici et al. (2013)
Left Bottom - Moreira et al. (2017), Right Bottom - Cunha et al. (2010)

The earliest work in the area of MRI based prostate intervention was carried out by Chinzei et al. at the Brigham and Women's Hospital. They developed an MR compatible robot system for surgical assistance during prostate interventions. It was used under open MRI to guide probes and needles during prostate interventions and brachytherapy (Chinzei et al. (2000)). Bosch et al. were responsible for the development of a system which undertook the first human trial. They developed a 5 DOF system which was manually operable with an automatic needle drive (Van den Bosch et al. (2010)). Stoianovici et al. also developed a 3 DOF system for MRI guided endorectal prostate biopsy with their novel pneumatic stepper motors called Pneustep. Their experimental results showed that the robot was MRI safe and achieved results with accuracy in the order of 2 mm (Stoianovici et al. (2013)). Morreira et al. were also responsible for developing the MIRIAM robot for MRI guided prostate intervention. The MIRIAM robot is actuated by piezoelectric motors with pneumatic actuation used for the needle insertion mechanism (Moreira et al. (2017)). Cunha et al. also developed a 6 DOF system for prostate intervention called MrBot. MrBot was also used in clinical trials on human patients and gave promising results (Cunha et al. (2010)). Another prototype of an MRI conditional robot with piezoelectric actuators and integrated with a high-resolution fiber-optic sensor for prostate brachytherapy was presented by Su et al. The robot had 6 DOF capable of steering inside a 3T MRI scanner. The needle drive mimicked the manual physician's gesture by two-point grasping. Experimental tests were conducted to measure the SNR loss, needle steering capacity, and fiber optic sensing range (Su et al. (2011)). Bomers et al. worked with the Remote Control Manipulator by Soteria Medical BV (Arnhem, the Netherlands) to assess its feasibility to perform transrectal prostate biopsy. The robot was pneumatically actuated and deemed MRI safe. 20 patients underwent RCM aided prostate biopsy with promising results (Bomers et al. (2017)).

2.3.4 Breast

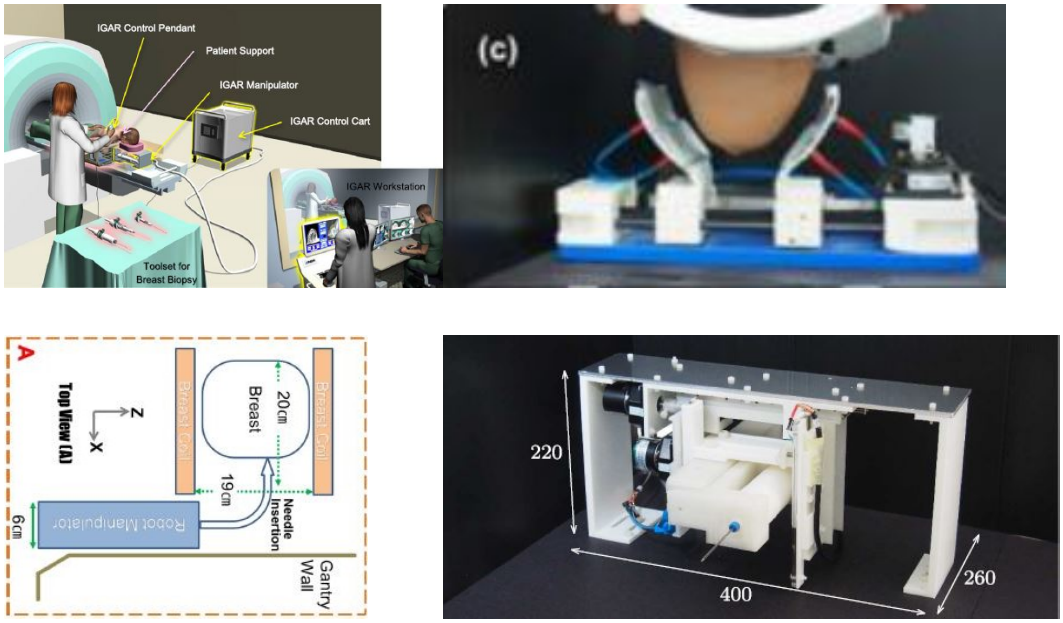

Figure 2.10: Left Top - Chan et al. (2016), Right Top - Zhang et al. (2016)
Left Bottom - Park et al. (2017), Right Bottom - Navarro-Alarcon et al. (2017)

Early study over robotic systems for breast interventions took place in the United States and since then many systems have been developed in this area. Yang et al. developed a unique 6 DOF robotic platform with a 1 DOF needle driver. The system was developed in two modules i.e. a master module outside the MRI scanner and a slave module inside the MRI scanner. In this system, pneumatic cylinders were used for actuation (Yang et al. (2014)). The IGAR (Image-guided automatic robot) platform was developed by Chan et al. for performing highly accurate clinical interventions under image guidance. The IGAR robot is MR conditional and system tests in air were reported (Chan et al. (2016)). Another unique system, developed by Zhang et al., was a palm-shaped breast deformation device that could be used to immobilize the breast for manual intervention. The device was capable of operating inside the bore of the MRI scanner along with image feedback (Zhang et al. (2016)). Park et al. developed an image-guided intervention robot system that was capable of operating inside the MRI gantry. The limitations of space inside the bore of the MRI scanner were overcome by incorporating a bendable needle in the robot. The system was almost automatic, in a way that the operator only chooses the target point from the MRI image and the robotic system automatically controls the needle and drives it up to the target point (Park et al. (2017)). Navarro - Alarcon et al. developed a new 3 DOF robotic system for MRI guided breast biopsy. The robotic system was MR conditional and it was actuated using a combination of piezoelectric and pneumatic actuators. The needle insertion was controlled using an adaptive position regulator based on different position sensors (Navarro-Alarcon et al. (2017)).

2.4 Automatic Trajectory Planning

There have been multiple attempts to make the medical and MRI based robots automatic and some research has been done in the area of automatic trajectory planning for these robots. Various methods have been used for robots to reach their target which have been discussed in this section.

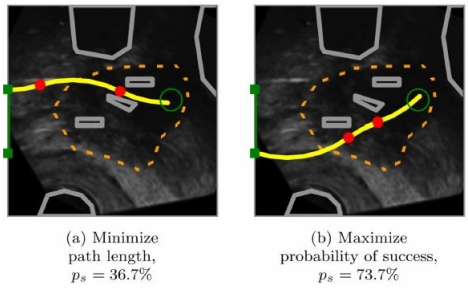

(a) Minimize path length, $p_s = 36.7\%$

(b) Maximize probability of success, $p_s = 73.7\%$

Figure 2.11: Path planning maximizing the probability of success (Alterovitz et al. (2008))

Alterovitz et al developed a new motion planning algorithm for a variant of a Dubins car with binary left / right steering and applied it to steerable needles, which were a new class of flexible bevel-tip needles which can be used to steer through soft tissue. Their method explicitly considered the uncertainty in motion due to patient differences and movement. The method was structured in such a way as to maximize the probability of the needle to reach the target rather than following the shortest path or other such criterias. Based on a segmented medical image with target and obstacles, their method formulated the problem as a Markov decision process based on the efficient discretization of the state space, modeling of motion uncertainty using probability distributions and planning the needle steering using dynamic programming. Their method was based only on parameters that could be extracted from images and they reported lab trials and the corresponding results (Alterovitz et al. (2008)).

Another path planning algorithm for image-guided neurosurgery was developed by Vaillant et al. They developed an algorithm for finding optimal needle insertion paths in the brain. Their algorithm was based on computing a cost function for every entry point on the outer boundary of the brain which was a possible candidate entry point. Since the brain is a critical organ, information about critical areas in the brain such as thalamic nuclei, optic nerve, and individual Brodman's areas were taken into account while selecting the candidate entry points by the algorithm. Their algorithm computes the cost of the path associated with the critical structures as well as the cost of the total path to the target however the final choice needs to be made by the surgeon (Vaillant et al. (1997)).

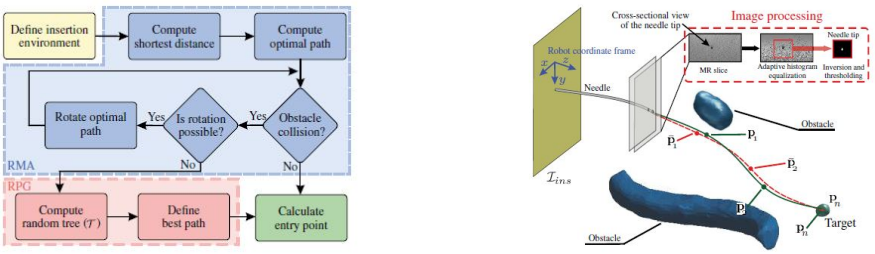

Figure 2.12: Left - Automatic operation Procedure (Moreira et al. (2017))
Right - Path planning sample (Moreira et al. (2017))

Morreira et al. developed the MIRIAM robot for MR guided interventions in prostate for procedures such as prostate biopsy and brachytherapy. The MIRIAM robot had a combined 9 DOF with 5 DOF given to the parallel robot while the needle guide had 4 DOF to insert, rotate and fire the needle during the procedure. The needle entry point was calculated based on the needle deflection model and the location of the obstacles and the target. They made use of the Rotation Minimization algorithm (RMA) to find the shortest path to the target based on the

kinematics of the needle deflection. If the RMA cannot find a suitable path, then the random path generator (RPG) algorithm was used to find a suitable path. In both approaches, their algorithm computes the path in such a way that the target is always reached irrespective of the cost to reach the target (Moreira et al. (2017)).

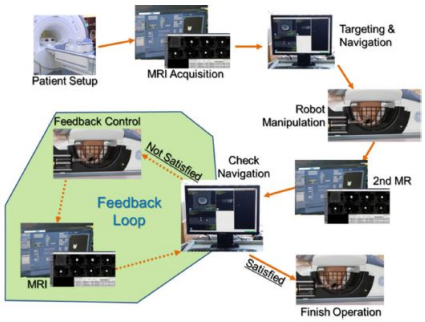

Figure 2.13: Process Overflow (Park et al. (2017))

Park et al., in their paper on image-guided breast needle intervention robot system, also develop an MR compatible robot that incorporates automatic path calculation. The doctor chooses the target and the developed software calculates the needle's navigation and visualizes the needle path. The Image sets from the MRI are transferred to the software and here the clinician can view and choose a target point. Image segmentation and template matching softwares are used to detect the current position of the needle and the geometry of the breast. The software then displays a path and the clinician can confirm the path by checking the presence of any risk factors (Park et al. (2017)).

The Image-guided automated robot (IGAR) is a robotic manipulator intended for MRI guided breast biopsy procedures developed by Chan et al. The software provides the ability to the user to choose a target point from the given images. The software calculates any potential interference with the grid or sides and prompts for any issues. If any issue, their system has the ability to go into fail-safe mode and any further operation is stopped (Chan et al. (2016)).

2.5 Evaluation Methods

Since there can be multiple ways a certain system can be evaluated, it is important to have an overview of the evaluation methods used while evaluating automatic robots. This can be helpful later in choosing the most ideal method for the system developed under this project.

In the case of the system developed by Alterovitz et al., the path planning software was developed on C++. The system was modeled in such a way that the probability of success is maximum irrespective of the cost of the path. Of course, the probability of success depended on the uncertainties in needle motion due to unavoidable needle tissue interactions or bending. Since the system used dynamic programming, the DP lookup table provided reliable values for initial insertion location, orientation, and bevel direction. The combination that maximized the probability of success was chosen. After each stage, the current position of the needle was obtained and thus the discretization error was reduced. The discretization error was further considered by the path planner as well. Since the computational complexity of the motion planner was $O(kN^2)$, fewer than 300 iterations were required for every example. For every example, varying values were chosen for parameters such as radius of curvature, workspace size, and discretization parameters. Computation time to solve the MDP ranged from 67 sec to 110 sec. However, the computation is always performed pre-operation. Once the computation was complete, the actual operation time was quite reasonable since it only

involved looking up the DP table for the path planner (Alterovitz et al. (2008)).

Vaillant et al. evaluated their system by choosing the VPL thalamic nucleus as their target region. Critical structures were defined and the target within the region was chosen manually from the 3D dataset. The OpenGL graphics library was used to develop software that could extract the outer surface region of the brain. Smoothing filter was then applied to the critical structures and the cost was computed for every insertion point in the brain. It took a combined time of 30 min and 30 sec for registration of the brain and computing the cost. The resulting cost is then mapped onto the planar domain to characterize the brain into colored regions where bright areas indicate relatively safer areas. The results are then finalized after an agreement with the surgeon and a final path is then generated (Vaillant et al. (1997)).

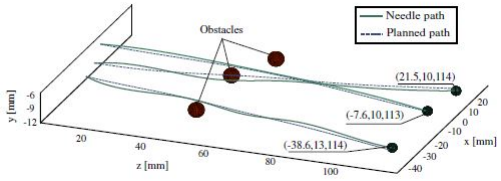

Figure 2.14: Evaluation Results MIRIAM Robot(Moreira et al. (2017))

Evaluation of the MIRIAM robot developed by Moreira et al. involved both in air and MRI based evaluation. The initial evaluation was done in air for the accuracy of the needle guide placement. The 6 DOF probe was placed in the needle guide and moved to 20 different locations. The initial and final robot positions are computed for 100 samples and errors were computed for deviations in translation and rotation in all X, Y, and Z directions. The evaluation was further done in MRI as well and the MIRIAM robot has been classified MRI conditional due to the use of piezoelectric motors and encoders. The MRI scanner MAGNETOM Aera was used and a phantom was used for evaluation. The robot caused a maximum of 27 % drop in the SNR and lower than 2% passive global distortion and lower than 1% active global distortion in the images. A test was also done for geometric distortion by embedding 6 pins in a phantom at known locations and it was found to be negligible. Lastly, an experiment was performed for targetting accuracy by performing 6 needle insertions. The obstacles and target locations are defined by the user during pre-operative images. The figure above shows the obstacles and targets as well as the planned and actual path to the target. The tracking algorithm also uses the same imaging protocol and the average targeting error was found to be 1.86mm with a standard deviation of 0.48mm. The time required for completing a single insertion was found to be 25 min (Moreira et al. (2017)).

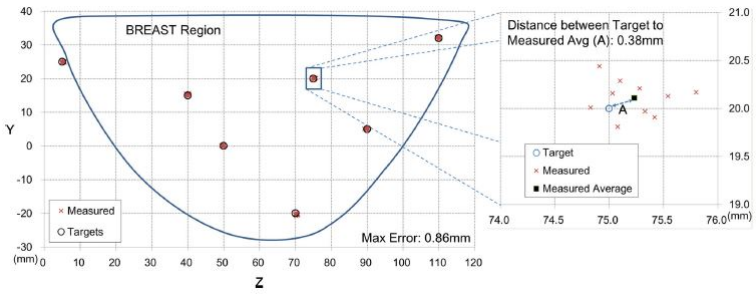

Figure 2.15: Evaluation Results showing max error 0.86mm (Park et al. (2017))

Park et al. used a breast phantom for their experiments to evaluate their robot inside the MRI scanner. SNR measurements were carried out in two steps - one with the motor placed inside

the breast coil with shielded wires to the controller and other when the motor was placed besides the breast coil. Tests revealed that the motor kept inside the breast coil gave poorer results as compared to when it was kept besides the coil. The evaluation for the targetting accuracy was done by initially calibrating the robot and then attaching 2 IR markers to it in order to track the robot during measurement. The measurement was done in two steps where the first step involved measurements in the YZ direction. The platform was positioned 10 times at 7 positions thus recording 70 measurements. The figure above shows the pictorial representation of the test. The differences in the Y and Z direction were found to be 0.06 ± 0.2 and 0.08 ± 0.3 respectively. The second part of the test involved measurement for needle targeting. This test again was repeated 10 times and the differences in the X, Y and Z directions were found to be 0.02 ± 0.2, 0.5 ± 0.3 and 0.5 ± 0.4 respectively. In case of MRI evaluation, a target point was chosen and the robotic system proceeded to insert the needle. The needle missed the target by a distance of 5 mm when no feedback was used. However, when feedback was used from another MRI scan, the needle reached a point 2.3 mm from the target (Park et al. (2017)).

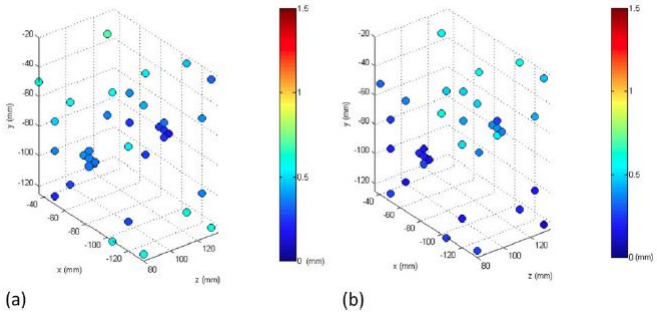

Figure 2.16: Evaluation Results showing the accuracy of 2 IGAR trial systems (Chan et al. (2016))

During the evaluation of the IGAR, Chan et al. conducted initial tests to test the safety and image distortion. Stepwise sequential images were taken by removing the IGAR components from within the room and comparing obtained results to standard known dimensions. For accuracy and repeatability tracking, a rigid test tool was driven to 34 target positions in free space inside the workspace. Following the test run, the kinematic model of the IGAR was corrected using a rigid body transformation. In order to test for repeatability, the entire 34 points were traversed twice by the IGAR system to check for repeatability. The figure above shows the accuracy results for the 2 systems and the color graph on the side represents the magnitude of error. Following calibration, the average accuracy error was found to be 0.40 mm and 0.34 for the 2 systems. Repeatability was found to be 0.2mm (Chan et al. (2016)).

Another important part of evaluation procedures is the evaluation of the biopsy samples taken. Groenhuis et al. performed the evaluation of biopsy samples by making using of staff-ink stained target lesions inside breast phantoms. Quality of biopsy samples taken was determined based on the proportion of ink stained material contained in the extracted samples. A sample was classified as successful if the ink stained portion in the sample was greater than 2mm (Groenhuis et al. (2020)).

2.6 The Stormram Series

Apart from the literature surveyed about the existing technologies and methods, the basis of this research comes from the preceding research which led to the development of the Stormram Robot series. Groenhuis et al. were responsible for the development of the entire stormram series which consists of 4 models or rather 4 stages of development. This current stage, the SUNRAM 5 is also the latest stage of their research.

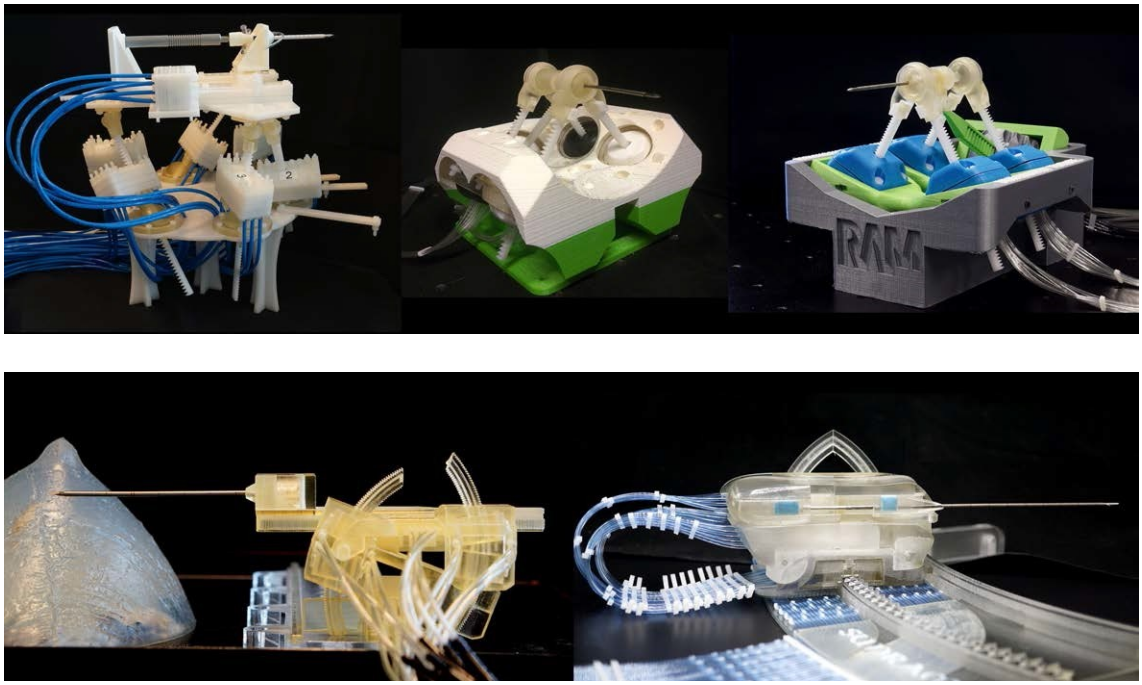

Figure 2.17: Top Row (L-R) - Stormram 1,2,3 (Groenhuis (2020))
Bottom Row (L-R) - Stormram 4, Sunram 5 (Groenhuis (2020))

2.6.1 Stormram 1

The Stormram 1 is the first robot in the Stormram series and is a 7 DOF MR safe breast biopsy robot which is actuated using 7 linear pneumatic stepper motors. The inspiration for the design has been drawn from a Stewarts platform, a hexapod that has 6 DOF, and a needle installed on top of the platform which has an additional DOF. The pneumatic linear stepper motors work with 3 toothed pistons which can be actuated individually in a 3 phase fashion so as to accomplish the movement of the rack. A specific sequence of actuation is required in order to make the move towards either the left or right. Also, the links of the hexapod (vertical rods) are connected to the main body frame using ball and socket joints. These joints are responsible for providing rotational motion to the platform. Also, there is no rudimentary degree of freedom so that the orientation of the stepper motor is fixed and collisions can be avoided (Abdelaziz et al. (2017)), (Abdelaziz (2016)).

2.6.2 Stormram 2

The earlier developed Stormram 1 was bulky and not computer-controlled. The Stormram 2 was precisely developed to tackle these 2 issues. The robot was developed to be MR safe i.e. fully out of plastic components driven by pneumatic linear stepper motors also fabricated in plastic. The Stormram 2 has 2 main parts viz. the main robot frame and the needle holder. The needle holder is connected to the frame of the Stormram 2 using a five link parallel platform. Every link connects a ball joint in the frame to a joint on the needle holder. The movement of the links between the joints is controlled using the pneumatic stepper motors.

Pneumatic linear stepper motors are used to actuate the links in order to move the robot. The three pistons in the motor move up and down individually, according to the pressurization waveform of the six chambers to make the rack of the motor move in the desired direction. The sequence of actuation of the pistons can be decided in order to actuate the rack in the desired direction. Multiple steps can be performed in either direction by applying appropriate

waveforms to the six chambers. The needle holder holds the titanium needle. The robot was able to target the lesion with an accuracy of about 6mm and the process was completed within 31 minutes (Abdelaziz et al. (2017)), (Abdelaziz (2016)), (Groenhuis (2020)), (Groenhuis et al. (2016)).

2.6.3 Stormram 3

Similar to the Stormram 2, the Stormram 3 is also an MR safe robot which can perform MR guided breast biopsies. The total dimension of the robot base is 160 x 180 x 90 mm. The method of actuation is the same as before i.e. using pneumatic linear stepper motors and these are driven by a valve manifold which is then placed outside the Faraday cage of the MRI scanner. Like the Stormram 2, the Stormram 3 is also a five-link parallel manipulator. It has a base and 5 carriers for the 5 links connected to the main needle holder. All parts are rapidly prototyped using 3D printing.

The linear pneumatic stepper motors are unique motors designed by Groenhuis et al. themselves and are pneumatically operated. The stepper motor's inner design consists of toothed pistons on which the rack can slide. By pressurizing selectively, the direction of movement of the rack can be controlled. By mounting vertically, the racks can be moved to cause upward and downward motion. By selectively pressurizing the six chambers with appropriate waveforms, the position of the rack can be controlled in steps of 0.67 mm. The needle holder consists of seven pieces also all 3D printed and rapidly prototyped. The central shaft consists of 2 parts connected by a Bayonet mount and can hold a 12 gauge needle. There are two more combined ball/revolute joints and the sockets are attached to the racks of the stepper motors forming the links. The 5th rack used for linear translation of the needle holder is connected to two parts which are pin joints.

The Stormram 3 incorporated a pneumatic distributor to selectively control the pressure waveforms supplied to the linear stepper motors. A manually controlled distributor was used earlier however since it would have been almost impossible to guide a needle only using visual servoing, the Stormram 3 had a computerized valve manifold. The manifold is used to drive the stepper motors in turn controlling the robot only in feedforward fashion. The manifolds are placed outside the Faraday cage and connected to the robot using thin tubes.

Several experiments were performed to analyze the performance of the joints and the two types of motors as well as to assess the repeatability of the Stormram 3. The pin joints did not suffer from any backlash. However, there was some small parasitic movement and a little friction. The repeatability tests were performed in air using the manual valve manifold and the repeatability was found to be better than 0.5mm. Further tests were also performed in MRI using the automatic valve manifold and the average targetting error was found out to be around 6mm. All in all, it was concluded that the Stormram 3 was a significant improvement over its predecessors. Further steps of development were in the areas of an automatic needle firing mechanism, a comfortable patient bed and breast mounting system, a software that combines preoperative MRI scans with a needle path planning system followed by post-insertion validation, and all this while taking into account breast deformations (Groenhuis (2020)), (Groenhuis et al. (2017)).

2.6.4 Stormram 4

The Stormram 3 was designed to improve the performance of the previous robots and also reduce the bulkiness of the whole system. However, all of the earlier developed robotic systems were parallel kinematic chains and although parallel kinematic chains make the system structurally rigid, they also limit the workspace and make forward and inverse kinematics relatively

complicated. Therefore, the thought was to develop a new robotic system, the Stormram 4, with a serial kinematic chain which could be driven by a combination of unique linear and curved pneumatic stepper motors. The challenge here was to preserve the structural rigidity since the use of a serial kinematic chain provided several other advantages in terms of structural and kinematical complexity, controllability, and workspace requirements. The Stormram 4 is a 4 DOF serial kinematic needle manipulator. The 4 DOF involves lateral movement along the base rack in either direction, vertical movement as well as lateral movement in the direction perpendicular to the base rack. The last DOF comes from the rotation obtained during verticle movement due to the use of curved stepper motors. The 4 DOF are actuated by pneumatic stepper motors. Two unique stepper motors have been used in the Stormram 4 viz. the T-26 linear stepper motor and the C-30 curved stepper motor. Like the Stormram 3, the Stormram 4 is also controlled using a pneumatic valve manifold. The controller used to control the FESTO valves is the Arduino Mega Board. The user can control the movement of the robot and additionally the stepping frequency as well as a few other advanced actions.

Various experiments were performed with the Stormram 4 to validate the performance of the stepper motors as well as to test the needle tip accuracy measurements. The in-air positional accuracy was evaluated using a sheet of paper, placed on the Y plane, on which 7x5 targets were drawn with 25mm separation. The robot was pre-programmed to move to these targets in succession and this resulted in a puncture in the sheet. The final standard deviation was observed to be 0.20 mm and the accuracy in Y direction was 0.2 mm. The experiment was re-performed and the repeatability was observed to be better than 0.1mm. Additionally, the robot performance was also tested in the MRI environment. However, since the coordinate system in MRI and the robot coordinate system are different, a coordinate transformation was defined in 3D. MRI accuracy tests were then conducted using breast phantoms and 30 sites were identified in the transform. The controller was placed outside the Faraday cage of the MRI and the valves were connected with 5m long tubes. The average targetting error (shortest distance to the target) was found to be 1.29±0.59 mm without considering the insertion depth and 1.87±0.8 mm after considering the insertion depth. In the end, it was observed that errors in X and Z direction were comparable however when the insertion depth was considered, a significant bias of about 0.73 mm was observed and a similar bias of about 0.44° was observed in the angle of orientation.

In the end, it was concluded that the Stormram 4 had demonstrated the ability to manipulate a needle towards a target with submillimeter accuracy and precision. It was a significant improvement in the state of the art robots in terms of workspace, accuracy, size, and complexity. Further areas of development were identified as the use of a breast fixation system, use of a biopsy gun, improvement in structural stiffness, and incorporation of safety mechanisms (Groenhuis (2020)), (Groenhuis et al. (2018)), (Groenhuis et al. (2017)).

2.6.5 Sunram 5

The latest model in the series, the SUNRAM 5 is the 5th model in the series. The SUNRAM 5 is explained in detail in the next section.

3 SUNRAM 5

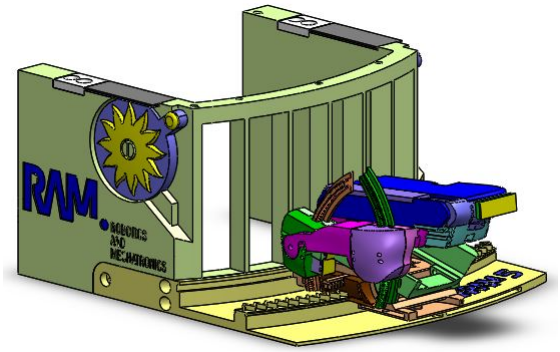

Figure 3.1: SUNRAM 5 mounted on the Machnet inspired Breast Fixation System

After the first 4 robots in the Stormram series, the SUNRAM 5 is the 5th generation robot in series. The SUNRAM 5 is a 5 DOF robot driven by six pneumatic linear and curved stepper motors and 3 single-acting cylinders. The SUNRAM 5 also has a Machnet inspired breast fixation system and an emergency needle ejection mechanism. Following from the Stormram 4, the SUNRAM 5 also has a serial kinematic chain.

3.1 Design and Implementation

3.1.1 Single Acting Cylinder

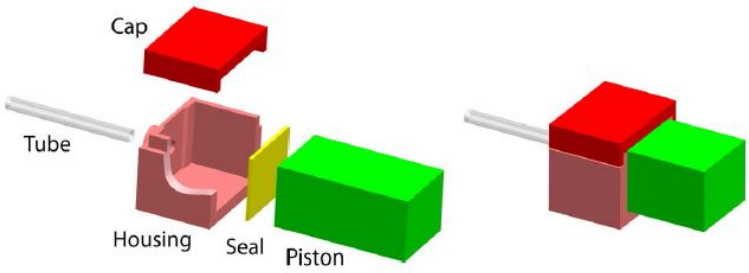

Figure 3.2: Single acting cylinder construction (Groenhuis (2020))

The single-acting pneumatic cylinder was used in the SUNRAM 5 robot. Pneumatic cylinders consist of a hollow cavity in which the cylinder piston can slide back and forth. Application of pressure in the cavity results in the generation of force which results in delivering work to the environment. The special property of the cylinders used here is that they are of rectangular cross-section as opposed to the usual circular cross-section ones. These cylinders are easily manufacturable with good accuracy. Since the cylinders are pneumatically controlled, an important part of the cylinders is the seal which is useful to block the escaping air. The cylinder is 3D printed in two parts - the base housing and the cap and the seal is laser cut from rubber. Like the single-acting cylinder which can only push the piston in 1 direction, a double-acting cylinder can also be produced. However, in this application, it was done simply by joining two single-acting cylinders opposite to each other. By supplying pneumatic pressure separately, they can be actuated in either direction (Groenhuis (2020)).

3.1.2 Stepper Motors

Figure 3.3: Left - Stepper Motor Architecture (Groenhuis (2020))
Right - Stepper Motor Operation (Groenhuis (2020))

A stepper motor can be produced by using multiple such double-acting cylinders that act on a toothed rack. The general mechanism of operation of these motors, which was not explained in any of the earlier sections, is being explained here. The internal architecture of the motors consists of a rack and 2 double-acting pistons with teeth like structure to engage with the rack. The pistons move inside the chambers and by selectively pressurizing the chambers with appropriate waveforms, the order in which the pistons move can be controlled thereby controlling the direction of movement of the rack. By design, the motor has zero backlash and non zero hysteresis (Groenhuis (2020)).

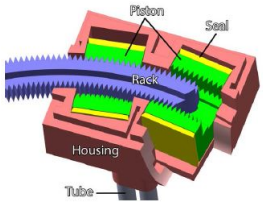

Figure 3.4: Curved Stepper Motor (Groenhuis (2020))

Like a linear stepper motor, a curved stepper motor can also be developed in which the rack, instead of being linear, is curved with some finite radius. The only difference here is that internally the 2 cylinders are not parallel but angled so that the piston movement is always perpendicular to the curvature of the rack (Groenhuis (2020)).

Dual-speed Stepper Motors

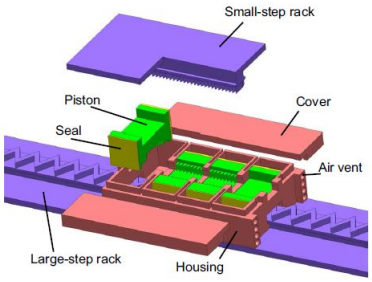

Figure 3.5: Dual-speed Stepper Motor (Groenhuis (2020))

Another special case of such stepper motors is the dual-speed stepper motor. Since there is a limit on the maximum frequency achievable inside the MRI, a tradeoff needs to be established between the time taken and the step size. Therefore, the solution developed here was to combine two or more stepper motors, with different step sizes, on the same axis to allow both high

speed and high accuracy movements. A dual-speed stepper motor is essentially a combination of two single-speed stepper motors with both motors using the same housing. The two racks of the stepper motors are at opposite ends of the housing to accommodate all cylinders of both stepper motors in line. The cylinders consist of pistons of which the center pistons support the smaller step size while the corner pistons support the larger step size of the rack thereby actuating sequentially and offering different step sizes and stepping speeds (Groenhuis (2020)), (Groenhuis et al. (2018)).

3.2 Kinematic Model

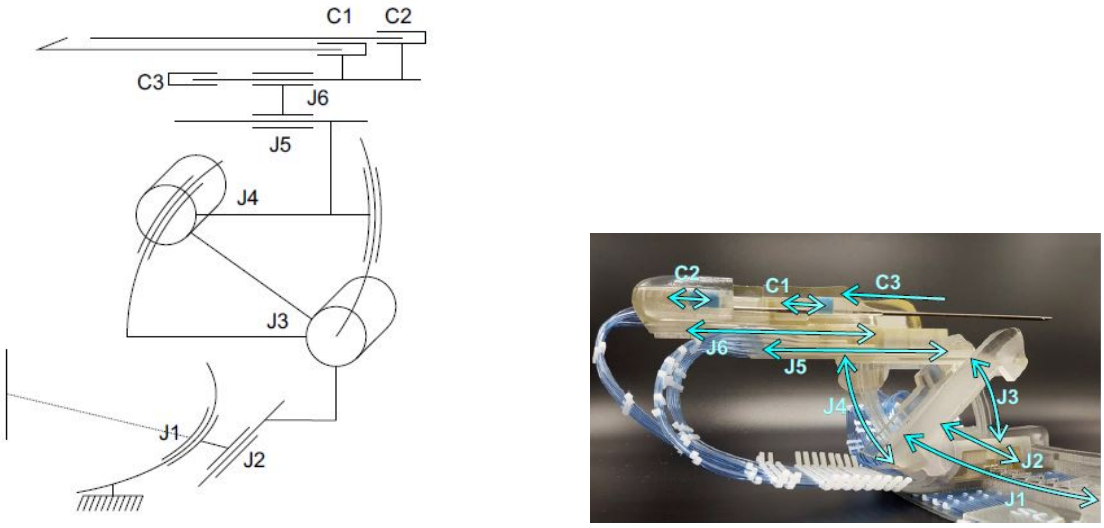

Figure 3.6: Left - Kinematic Model of the SUNRAM 5 (Groenhuis (2020)), Right - Pictorial representation of the joints in the SUNRAM 5 (Groenhuis (2020))

The SUNRAM 5 consists of six joints in total. Joint J1 is the curved rack at the base of the robot with a radius of 260 mm. The total angular distance is about 35°. The larger step size allows the coarse positioning of the robot and the angular movement is helpful in selecting a favorable insertion angle. Joint J2 is the linear stepper motor which is the second stepper motor at the base. It offers a range of 45 mm. Joint J2 allows fine lateral adjustments along with favorable insertion angles by circumventing the grating of the fixation system. Joints J3 and J4 are curved stepper motors that are used for lifting and tilting the needle holder. Both curved stepper motors have a step size of 0.3° with a range of 40°. Joint J5 is the linear stepper motor that is useful in moving the needle holder assembly forward and backward in small steps. It has a range of motion of about 50 mm which is used at the last stage to insert the needle after initial alignment. J6 is also a stepper motor along the same axis but with a larger step size and a range of motion of about 61 mm. Additionally, cylinder C1 is used to drive the inner needle of the biopsy gun over a range of 19mm and cylinder C2 slides the needle shaft of the inner needle over the same distance. C3 cylinder is used for the emergency needle ejection function.

3.2.1 Forward Kinematics

Forward Kinematics refers to the use of the kinematic equations of the robot to compute the position of the end effector from specified values of the joint configuration vector. In the SUNRAM 5, the forward kinematics converts the q vector to the coordinate point of the end effector in the inertial frame of the robot. The structure of the robot is divided into 8 motions (only a single motion at a time - either a translation or a rotation) and therefore 8 transformations to reach from the origin of the inertial frame to the end effector which in this case is the needle

tip. The simplest way to formulate the forward kinematic equation is as below.

$$p^0 = H_1^0 \cdot H_2^1 \cdot H_3^2 \cdot H_4^3 \cdot H_5^4 \cdot H_6^5 \cdot H_7^6 \cdot H_8^7 \cdot H_{ee}^8 \cdot p^{ee} \tag{3.1}$$

Here, of course, the H_i^{i-1} are the homogeneous transformation matrices to transform the coordinates from 1 frame to the next. Stepper motors of different step sizes (s1-s6) provide the motion and the q vector (q1-q6) defines the number of steps every stepper motor has to make in order to reach the desired configuration. The inertial frame 0 is the frame of the origin which is located at the centre of rotation of joint q1 and at the same height as the axis of rotation of q3. The origin as defined can be seen in the figure. The Z-axis is defined vertically and forms the height element while the X and Y axis form the horizontal flat plane.

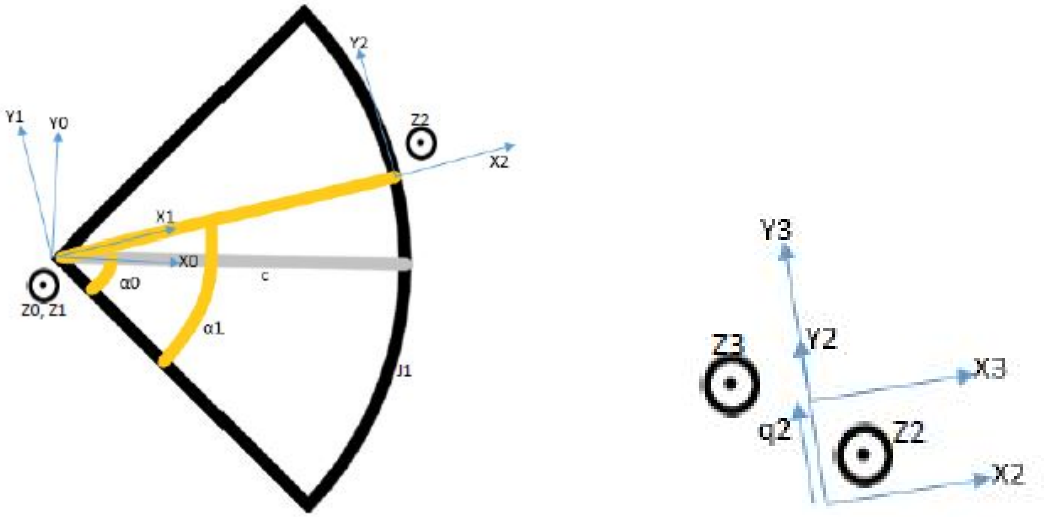

Figure 3.7: Left - Forward Kinematics Sketch 1 (Zwiep (2020))
Right - Forward Kinematics Sketch 2 (Zwiep (2020))

The first motion is to align the origin (frame 0) with frame 1 as shown in the figure. This forms the homogeneous transformation matrix H_1^0. Motion from frame 1 to frame 2 involves a pure translation. Frame 1 needs to be translated by a distance equal to c which is equal to the radius of the arc as can be seen in the figure. Homogeneous matrix H_2^1 includes only a pure translation. The third transformation in the XY plane includes a translation performed by the second stepper motor on the base. Although q2 is not zero when the displacement is zero, it is compensated due to the fact that the needle is off-center. The motion from frame 2 to frame 3 is also a pure translation. The magnitude of this translation can be defined in terms of the number of steps taken q2 times the step size s2. This forms the homogeneous transformation matrix H_3^2.

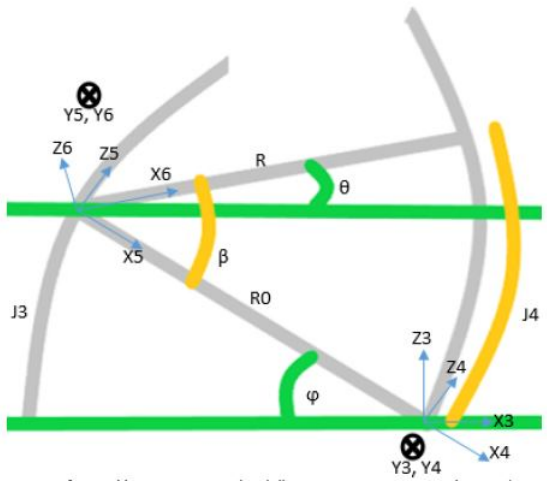

Figure 3.8: Forward Kinematics Sketch 3 (Zwiep (2020))

Once a complete transformation in the horizontal X Y plane is defined, the next part involves defining the vertical transformation in the Z direction. The 2 curved stepper motors (represented by q3 and q4) are responsible for the verticle movement. The figure shows how to visualize the motion from frame 3 to frame 6. The transformation from frame 3 to frame 4 denoted by H_4^3 is a simple rotation around the Y-axis. Correspondingly to move from frame 4 to frame 5, a translation is required by a distance equal to R0 as shown in the figure. This forms the homogeneous transformation matrix H_5^4. Lastly, to transform from frame 5 to frame 6 involves a rotation again around the Y-axis giving us the homogeneous transformation matrix H_6^5.

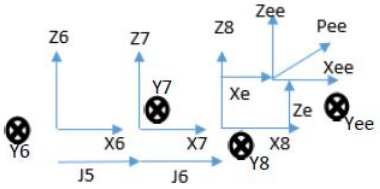

Figure 3.9: Forward Kinematics Sketch 4 (Zwiep (2020))

The last part involves the translations related to the needle holder assembly which again involves 2 stepper motors with two different step sizes (represented here by q5 and q6). Transformations from frame 6 to the end-effector frame only involve translations as can be seen in the pictorial representation. These three transforms give us the homogeneous transformation matrices H_7^6, H_8^7 and H_{ee}^8. Now once all the homogeneous transformation matrices are well defined and we have the complete forward kinematic equation, we can take the point $p^{ee} = (0 \quad 0 \quad 0 \quad 1)$ which is a 4x1 vector, and find out the coordinates of the end effector in terms of the origin coordinate frame while knowing the intermediate joint configurations. The complete forward kinematic equation is found to be as follows.

$$p^0 = \begin{bmatrix} \cos(\alpha) & -\sin(\alpha) & 0 & 0 \\ \sin(\alpha) & \cos(\alpha) & 0 & 0 \\ 0 & 0 & 1 & 0 \\ 0 & 0 & 0 & 1 \end{bmatrix} \cdot \begin{bmatrix} 1 & 0 & 0 & c \\ 0 & 1 & 0 & 0 \\ 0 & 0 & 1 & 0 \\ 0 & 0 & 0 & 1 \end{bmatrix} \cdot \begin{bmatrix} 1 & 0 & 0 & 0 \\ 0 & 1 & 0 & \text{q2}\cdot\text{s2} \\ 0 & 0 & 1 & 0 \\ 0 & 0 & 0 & 1 \end{bmatrix} \cdot \tag{3.2}$$

$$\begin{bmatrix} \cos(\alpha) & 0 & \sin(\alpha) & 0 \\ 0 & 1 & 0 & 0 \\ -\sin(\alpha) & 0 & \cos(\alpha) & 0 \\ 0 & 0 & 0 & 1 \end{bmatrix} \cdot \begin{bmatrix} 1 & 0 & 0 & -\text{R0} \\ 0 & 1 & 0 & 0 \\ 0 & 0 & 1 & 0 \\ 0 & 0 & 0 & 1 \end{bmatrix} \cdot \begin{bmatrix} \cos(\alpha) & 0 & -\sin(\alpha) & 0 \\ 0 & 1 & 0 & 0 \\ \sin(\alpha) & 0 & \cos(\alpha) & 0 \\ 0 & 0 & 0 & 1 \end{bmatrix} \cdot$$

$$\begin{bmatrix} 1 & 0 & 0 & -\text{q5}\cdot\text{s5} \\ 0 & 1 & 0 & 0 \\ 0 & 0 & 1 & 0 \\ 0 & 0 & 0 & 1 \end{bmatrix} \cdot \begin{bmatrix} 1 & 0 & 0 & -\text{q6}\cdot\text{s6} \\ 0 & 1 & 0 & 0 \\ 0 & 0 & 1 & 0 \\ 0 & 0 & 0 & 1 \end{bmatrix} \cdot \begin{bmatrix} 1 & 0 & 0 & -X_e \\ 0 & 1 & 0 & 0 \\ 0 & 0 & 1 & Z_e \\ 0 & 0 & 0 & 1 \end{bmatrix} \cdot \begin{bmatrix} 0 \\ 0 \\ 0 \\ 1 \end{bmatrix}$$

The SUNRAM 5 forward kinematics has been formulated by (Zwiep (2020)) as an individual project at the Robotics and Mechatronics department, the University of Twente.

3.2.2 Inverse Kinematics

Inverse Kinematics involves the mathematical process of calculating the joint configuration vector required to place the end effector of the kinematic chain in a given position and orientation with respect to the origin frame. In the SUNRAM 5, the end effector is the needle tip. Inverse Kinematics is aimed at calculating the corresponding joint configuration vector based on the desired position of the needle tip. However, it is not always useful only to use inverse kinematics since it does not guarantee a unique solution. In case of the SUNRAM 5, another major constraint with respect to the fixation system exists. The calculated joint configuration vector should be such that there should not be any collision between the robot and the fixation system frame.

In this case, the inverse kinematic equations are obtained by constructing many useful triangles to obtain the q vector. The q vector (q1-q6) here will give the number of steps to be taken by each motor so as to reach the desired position. An additional q7 term is used here which is a combination of q5 and q6. The steps to be followed, to find the inverse kinematic equation, are as follows.

1. Determine q1 and q2 without a collision check.
    - R_z is the rotation of the end effector wrt. the XY plane. X_{ee} and Y_{ee} are coordinates of the end effector.
2. Determine the updated q2 due to fixation system frame constraints.
    - Collision check is used. The orientation angle remains the same as before and the only change is in position.
3. Determine q3, q4, and q7.
    - q7 is a combination of q5 and q6 i.e. the steps of the needle guide motors. Z_{ee} is the coordinate of the end effector.

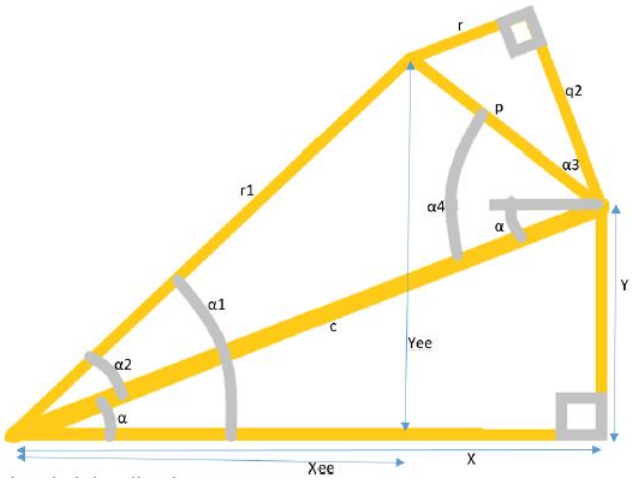

Figure 3.10: Inverse Kinematics Sketch 1 (Zwiep (2020))

In the figure shown above, three triangles are visible. This figure is used in computing q1 and q2 without considering the collision. We know X_{ee}, Y_{ee}, and Rz rotation of the end effector. By using standard Pythagoras theorem and trigonometry, we find out the kinematic equations for q1 and q2.

$$q_1 = \frac{(\alpha + \alpha_0) \cdot c}{s_1} \tag{3.3}$$

$$q_2 = \frac{p \cdot cos(\alpha_3)}{s2} \tag{3.4}$$

Now since the values for q1 and q2 have been found, a collision check can be implemented to check the fixation system frame constraints. 3 methods were used in order to perform the collision check.

1. Check if the line r intersects with any of the 3 lines around the frame. Endpoints of each frame line are measured in Solidworks.

2. Check if the line r intersects with a circle around each pillar of the frame. The midpoint of the circle is located using Solidworks.

3. Check the distance line r and center of each pillar in the frame. The center of the frame pillar has already been measured from Solidworks.

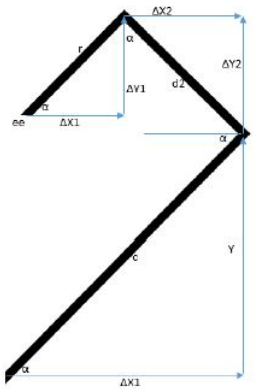

Figure 3.11: Frame Constraint Derivation (Zwiep (2020))

The most important part here is to determine the line r. Only the endpoints of the line need to be determined since the points inbetween can be interpolated. The equations used to determine these endpoints are as follows.

$$X_0 = X - d_2 \cdot sin(\alpha) \tag{3.5}$$

$$Y_0 = Y + d_2 \cdot cos(\alpha) \tag{3.6}$$

$$X_1 = X_0 - r \cdot sin(\alpha) \tag{3.7}$$

$$Y_1 = Y_0 + r \cdot sin(\alpha) \tag{3.8}$$

Once the line r was determined, a practical implementation of the 3 different types of collision checks showed that the third method of adjusting q2 with an orientation angle α gave the best results in the quickest time. And therefore only method 3 has been used.

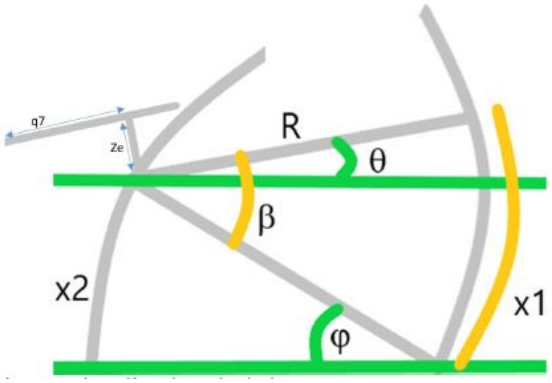

Figure 3.12: Inverse Kinematics Sketch 2 (Zwiep (2020))

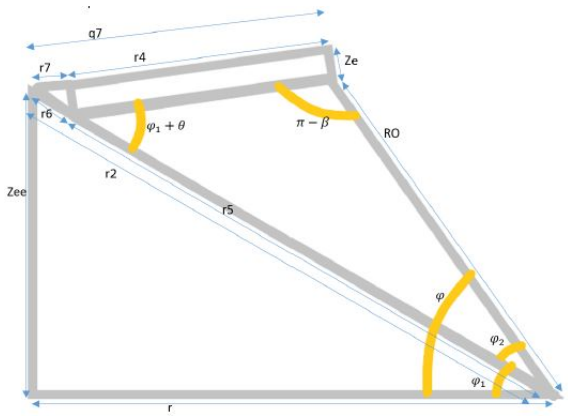

Figure 3.13: Inverse Kinematics Sketch 3 (Zwiep (2020))

The last part involves finding the values of q3, q4, and q7. The two given figures are used here. Here, the rotation of the end effector with respect to the XY plane R_{xy}, r, and Z_{ee} are known. The combined temporary value q7, which is a combination of q5 and q6, is used. Again, by using the Pythagoras theorem and trigonometry, it is possible to completely find the values of q3, q4, and q7.

$$q_3 = \frac{\phi \cdot R_0}{s_3} \tag{3.9}$$

$$q_4 = \frac{\beta \cdot R}{s_4} \tag{3.10}$$

$$q_7 = r_7 + r_4 - X_e \quad where \quad q_7 = q_5 \cdot s_5 + q_6 \cdot s_6 \tag{3.11}$$

This completes the complete derivation of the inverse kinematic equations required for the SUNRAM 5 robot. The SUNRAM 5 inverse kinematics has been formulated by (Zwiep (2020)) as an individual project at the Robotics and Mechatronics department, the University of Twente. The implementation of these kinematic equations is explained in an upcoming section.

3.3 Mechanical Design

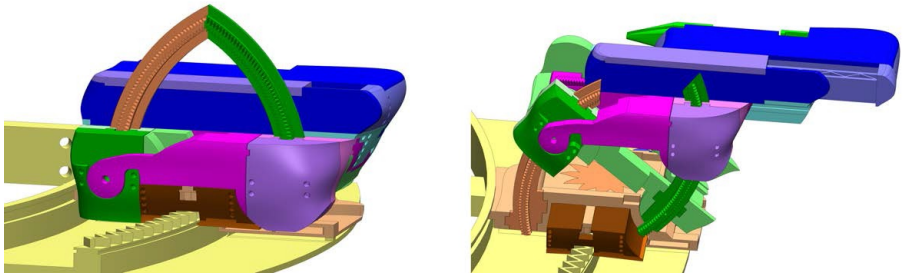

Figure 3.14: CAD Drawing SUNRAM 5 robot (Groenhuis (2020))

The above figures show the CAD drawings of the actual body of the SUNRAM 5 robot in standard and extended configurations. The robot has in total 16 pneumatic cylinders required for six singular stepper motors, two double-acting cylinders, and one single-acting cylinder. The total height of the moving parts of the SUNRAM robot excluding the base rack and cables is 47mm (Groenhuis (2020)).

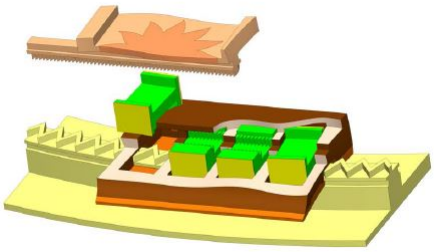

Figure 3.15: Base Rack (Joint J1 and J2) (Groenhuis (2020))

The base rack forms the dual-speed stepper motor consisting of joints J1 and J2 (step sizes 1.7mm and 0.3mm respectively) with the only difference that J1 is a curved stepper motor. Therefore, the base rack has 2 outer cylinders at a curved angle with respect to the 2 inner cylinders. The 2 joints in combination provide lateral translational movement along with a minor rotation with the axis almost at infinity. The upper joint J2 is mostly used for fine lateral adjustment to avoid the frame gratings (Groenhuis (2020)).

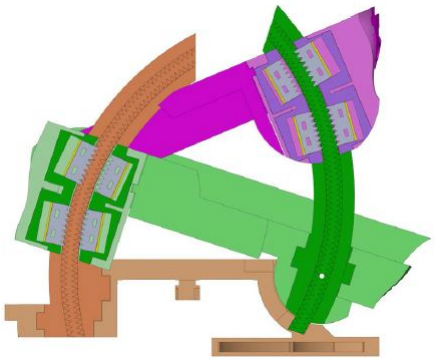

Figure 3.16: Vertical Lift and Tilt (Joint J3 and J4) (Groenhuis (2020))

The vertical lift and tilt motions are provided by the joints J3 and J4 which are curved stepper motors. The racks have a radius of curvature of 62mm and are hinged about acrylic pins in the axis of rotation.

Mounted on top of the vertical joints is the needle holder. The needle holder provides lateral translation movement with a dual-speed stepper motor. Additionally, it also consists of two dual-acting cylinders that are used for firing the biopsy gun along with a single-acting cylinder used for emergency ejection of the needle (Groenhuis (2020)).

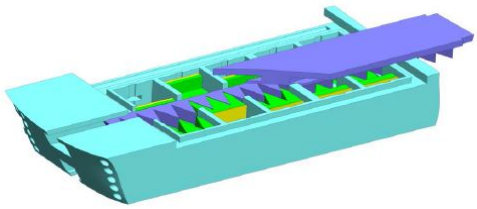

Figure 3.17: Needle Holder (Joint J5 and J6 with cylinders C1, C2, and C3) (Groenhuis (2020))

The needle holder has a combined five cylinders with three cylinders having step sizes 1.7mm and two cylinders having 0.3mm. These cylinders in combination provide a telescopic movement (translation). This expansion can be used for avoiding the frame gratings. Additionally, a single-acting cylinder is attached to the large step stepper motor for the emergency ejection mechanism. Two dual-acting cylinders with asymmetrical piston head sizes are used for the movement of the biopsy gun mechanism (Groenhuis (2020)). The default needle is a 14G 100mm needle which has been modified as a pneumatic biopsy gun. The only parts used from the original biopsy gun are the inner and outer needles then modified into a pneumatic biopsy gun.

3.4 Control Interface

Every pneumatic cylinder is controlled individually 5/2 type valve of Festo MHA2-MS1H-5/2-2 located in the valve manifold of the controller placed outside the Faraday cage of the MRI scanner. It is connected using 5 m long pneumatic tubes. To specifically control the airflow, the diameter of the tubes is 3-4 mm normally and 2 mm during the last 0.5 m. This is done to provide flexibility to various DOF's. It is not advised to use tubes with 2mm diameter for the entire length as it can constrict the airflow thereby reducing output. SUNRAM 5 consists of 16 pneumatic cylinders and thus 31 tube connections (since 1 cylinder is single acting so only 1 tube connection).

Figure 3.18: Arduino Controller with User Interface (Groenhuis (2020))

The Arduino controller is used as the main controller in the valve manifold. Additionally, the control interface also contains a pressure adjustment knob, internal pressure tanks, an emergency stop button, sliders for position control of the robot, and a display screen. There are also connections available for power, air supply, and USB. The control method used for controlling the SUNRAM 5 is only feedforward. The SUNRAM 5 does not have any sensors or any other form of feedback involved. Ideally, this is sufficient if the initial position is known and thereafter it is checked that no steps are skipped. The calibration is done at every iteration which involves operating the robot to the origin or starting point. Steps can be tracked thereafter either visually or by ensuring that the motor forces exceed the joint forces by a safety margin. Stepping frequency can also be controlled in order to change the speed of operation.

In the clinical workflow, the SUNRAM 5 has a fixation system to fix the breast and the robot-MRI coordinate transformation is defined using markers that are embedded in the fixation system. The target coordinates are then available in the robot coordinate system and the joint configuration is automatically calculated. The joint configuration can be automatically fed to the Arduino controller and the Arduino controller automatically operates the valves so that the robot moves to the target point. A confirmatory MRI can then be done in order to check the needle position and thereafter the biopsy gun can be fired to take the sample (Groenhuis (2020)).

3.5 Stepper Motor Evaluation

An individual evaluation of the stepper motors used in the SUNRAM 5 for their force and stepping frequency was already carried out by Dr.Groenhuis in his thesis (Groenhuis (2020)). The process is described here for clarification.

3.5.1 Evaluation of Stepper Motor Performance - Force

Ideally, the output force of a pneumatic piston can be calculated as the product of its cross-sectional area and the system pressure. Since the piston, in this case, reacts with a rack by means of a wedge mechanism, force is transferred with specific leverage. The actual force is, of course, lower because of the friction between the sliding components. An experimental apparatus was designed such that the stepper motor was made to lift weights and force was calculated as a function of pressure and stepping frequency.

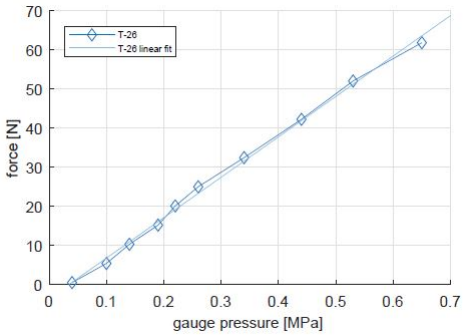

Figure 3.19: Stepper Motor Evaluation (Groenhuis (2020))

The graph shows a good linear relationship between the force generated as a result of the pressure applied with a maximum force of 62N at a pressure of 0.65MPa. Keeping in mind the cross-sectional area and the leverage factor, efficiency was close to 43%. Although this might seem low, even a pressure of 0.15MPa with a force of 11N is enough to move the SUNRAM 5 robot along all its axis except for firing the needle.

3.5.2 Evaluation of Stepping Frequency Performance

The maximum stepping frequency is an important factor since it determines until what frequency the robotic system can operate safely without skipping a step. It is mainly dependant on the length of the pneumatic tube inside the MRI environment. The air that flows through the tubes cannot exceed the speed of sound i.e. 343m/s. Additionally, the friction of air with the tube walls also plays a part. The volume of air flowing through the tubes is also limited based on the dimensions of the tube. The evaluation of the stepping frequency has also been performed by Dr. Groenhuis (Groenhuis and Stramigioli (2018)).

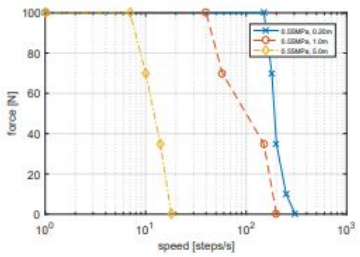

Figure 3.20: Stepping Frequency Graph (Groenhuis and Stramigioli (2018))

Since the motors used in the SUNRAM 5 and the stormram 4 are the same original models, ideally the maximum operating frequency of the motors when operating in free air should be the same as that evaluated for the stormram 4 i.e. up to 65 Hz. However, inside an MRI environment, the length of the tube is different i.e. at least 5m long. Therefore, this affects the maximum operating frequency of the stepper motors. The maximum frequency with which the stepper motors can operate inside an MRI environment is limited to about 10 Hz (due to the long length of the tubes) so as to generate the required force. In order to maintain this condition, all the actual experimental evaluations for the SUNRAM 5 were performed at a stepping frequency of 10 Hz.

4 Analysis and Implementation

This chapter covers the research methodology used while undertaking the research and its eventual implementation in designing an experiment for the evaluation. The detailed experimental design is also included here followed by the evaluation criteria as well.

4.1 Research Methodology

The primary research question underlining this study was 'How does the SUNRAM 5 evaluate with respect to its predecessor, the Stormram 4 ?'. The answer to this research question ideally was a comparative evaluative study that provides insight into the performance of the robot based on certain predefined parameters as well as the functionality of the robot in a full clinical biopsy procedure. This would have eventually then allowed to draw conclusions based on the comparison between the evaluation results of the SUNRAM 5 and the Stormram 4.

The aim of the study was to initially define a full workflow for a clinical breast biopsy procedure using the SUNRAM 5 and evaluate the performance of the SUNRAM 5 during this procedure. Therefore, in order to establish the fact that the newly developed system was at least equal in performance or better than the earlier system, it was essential to evaluate the new system in terms of the performance of certain individual parameters, targetting accuracy evaluations similar to the earlier systems as well as the total performance evaluation in a full clinical biopsy procedure. This would have led to results which would have enabled the apt comparison between the SUNRAM 5 and the Stormram 4. The SUNRAM will, therefore, be initially evaluated for the performance of the dual-speed stepper motors as well as the targeting accuracy while operating in air. This will then be followed by evaluating the performance of the SUNRAM 5 in a complete clinical MRI based breast biopsy procedure based on MRI scans. Multiple iterations of measurement would prove the reliability of the result, its comparison, and the thereafter drawn conclusion.

4.1.1 Survey of Existing Data

Since the main area of research here was related to MRI safe robotic systems for breast biopsy, the focus of the research was mostly limited to breast biopsy and MRI safe robotic systems. However, since the main research question also involves evaluation, additional research was undertaken in the evaluation procedures used in MRI based systems related to biopsy, as well as automated systems for biopsy for future recommendations.

The start point of this research was the Ph.D. thesis of Dr. Vincent Groenhuis who is responsible for all the work undertaken in developing the Stormram robot series (Groenhuis (2020)). SUNRAM 5 is the fifth robot in the series which was the primary subject of this study. Initial references were all gathered by following the thesis and areas of referencing were defined. The study was started by initially looking into the areas of various imaging techniques, about the biopsy process and in detail about the MRI guided biopsy process. Furthermore, another main part of the literature gathering was covered by the Stormram robot series and the entire literature available related to it. This was then further followed by diving deeper into other existing state of the art robotic systems related to breast biopsy and in general robotic systems that were used in medical applications. Although the main research topic is related to breast biopsy, studying about other applications of robotic systems in other medical applications gave an insight into the state of the art capabilities of the robots and various experiments, criteria, and techniques used in evaluation and testing. Much help came from the paper by Monafaredi et al. which outlines various existing MRI based robotic systems and their applications in

various areas (Monfaredi et al. (2018)). This proved to be of huge help in gathering references. Lastly, the research was concluded by looking into the area of automated robotic systems that were used in MRI based interventions. This part was quite essential since it gave great insight into the algorithms used in other state of the art systems for path planning and navigation as well as actuation and control. This part was essential in drawing recommendations for future improvement.

4.2 Coordinate Systems

The correct definition of coordinate systems is an important part of this research. The standard MRI coordinate system uses the LPS (Left Posterior Superior) coordinate system with the origin at the magnet's isocenter. However, it is always difficult to exactly pinpoint the location of the magnet's isocenter. Therefore, it is necessary to define a coordinate system for identifying the lesion coordinates i.e. a defined MRI coordinate system. The robot coordinate system needs to be defined in order to translate the locations of the lesions (targets) from the defined MRI coordinate system such that it can be used to define the robot motion.

The inertial coordinate system also needs to be defined to work on the kinematics of the robot. This system can be either same as the robot coordinate system or different. However, since the kinematics of the robot was developed by (Zwiep (2020)) as a part of his individual project, the kinematics coordinate system was chosen differently. Therefore, the entire experimental procedures involve a lot of interchange between the three coordinate systems.

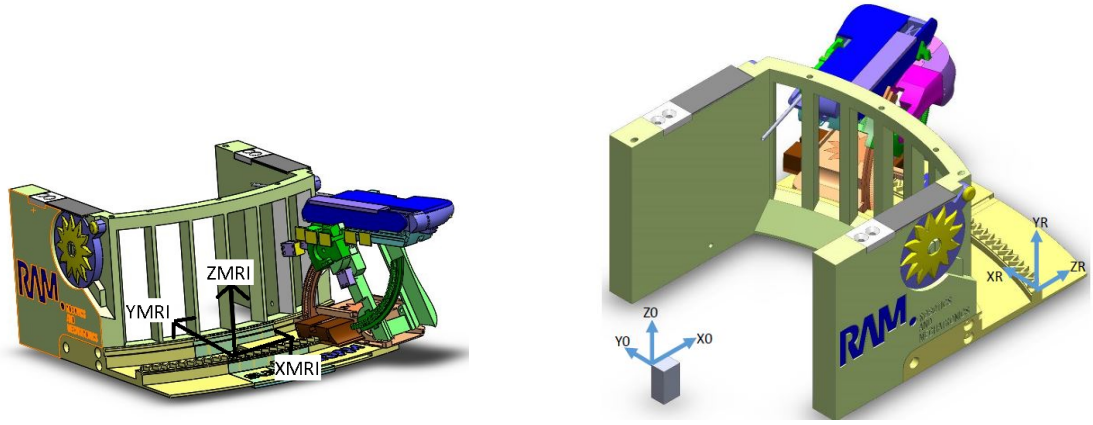

Figure 4.1: Left - The Location of the MRI coordinate System (Ψ_{MRI}), Right - The locations of the Kinematic Coordinate System (Ψ_0) and the Robot Coordinate System (Ψ_R)

The defined MRI coordinate system has been defined at the base of the centermost marker among the 5 markers embedded inside the SUNRAM 5 breast fixation system. The robot coordinate system has been defined at the left-most point on top of the curved base rack which is kind of symbolic to the start point of the robot. On the other hand, the kinematic coordinate system, inertial frame for the robot kinematics, has been defined at a location which is at the axis of rotation of the curved base rack (motor q1) and at a height equal to the axis of rotation of the front lifter motor (motor q3). Figure 4.1 - Right gives a visualization of the kinematic coordinate system (X0, Y0, Z0) and the robot coordinate system (XR, YR, ZR).

4.3 Segmentation and Registration

In standard DICOM images of MRI scans, the LPS (Left Posterior Superior) coordinate system is used with the origin at the magnet's isocenter. The LPS coordinate system is defined with respect to the patient who is being scanned i.e. either the left or right of the patient, the anterior

or the posterior of the patient, and the inferior or the superior of the patient. Since it is difficult to accurately pinpoint the location of the origin of the LPS coordinate system, an MRI based coordinate system has been defined as shown in Figure 4.1. However, the robot naturally uses the XYZ coordinate system with the origin at a different location. Therefore, the targets or the lesions which are identified in the MRI Coordinate System are located with respect to the LPS coordinate system and thus need to be transformed to the robot coordinate system Figure 4.1. The associated coordinate transformation is defined using the 5 markers embedded inside the fixation system of the SUNRAM 5.

The MRI scans were made inside the 0.25 T (G-Scan, Esaote SpA, Genoa, Italy) MRI scanner. The MRI scanner was geometrically calibrated using a custom 3D grid pattern (cube) in order to compute the geometric distortion. A 5th order correction function was developed in order to take into consideration the geometric distortion (Groenhuis (2020)). A 3D Hyce scanning sequence was used as the scanning protocol with parameters TR=10 ms, TE=5 ms, and FA=0°. The scanning direction was the coronal plane.

Figure 4.2: 3D volume reconstruction of MRI scans

An automatic marker registration method was used to register the location of all five markers as are visible in the MRI scan. Initially, the markers are extracted on the basis of the total volume of connected components in a geometrically corrected binary scan. Based on a distance matrix constructed by taking the actual physical distances between the markers, the intra-marker distance is considered and the five markers are identified. Based on the centroid locations of these 5 markers, a best fit rigid 2D transformation in the flat plane is constructed. After combining with the posterior component, the 3D coordinate transformation is now fully defined. All values are expressed in the robot coordinate system Figure 4.1.

Target	Expected Registered Position (mm)			Actual Registered Position (mm)		
1	134.7	53.8	-84.7	136.5	52.8	-84.7
2	88.5	58.8	-86.3	90.4	59.1	-86.3
3	108.5	60.7	-81.7	110.5	60.4	-81.7

Table 4.1: The expected and achieved registration accuracy from segmentation of the MRI scan

Evaluation showed that the target coordinates were registered with an average error of 1.93mm in the X direction, 0.51mm in the Y direction and 0mm always in the Z direction as per the robot coordinate system Figure 4.1.

4.4 Experimental Evaluation

The main aim of this research study is the evaluation of the SUNRAM 5 and the comparison of its performance with the earlier editions of the robot. Dual-speed stepper motors are one of the new additions to the robot over its earlier versions. A theoretical evaluation is intended to be performed for the positioning accuracy of the dual-speed stepper motors and a practical evaluation will be performed for the operating time. An evaluation for the targetting accuracy is also intended to be performed in 2 experimental environments viz. in air and inside an MRI scanner. Since the robot is intended to be used inside the closed bore MRI scanner, the spatial compatibility of the robot inside a closed bore MRI scanner will also be evaluated. A small evaluative study will also be put out for depicting the reachable workspace by the needle tip. Lastly, a full MRI-guided biopsy workflow is defined and the procedure time using the SUNRAM 5 is evaluated. The detailed experimental evaluation process is explained in this section. In all the experiments described, the coordinate system used is the robot coordinate system Figure 4.1.

4.4.1 Evaluation of Dual-speed Stepper Motors - Operation Time and Positioning Accuracy

An experimental evaluation will be performed for evaluating the time required for the dual-speed stepper motors to reach a certain position. The base rack of the SUNRAM 5 as well as the needle guide both have been equipped with the dual-speed stepper motors (referred to as joints q1,q2 and q5,q6 in the kinematic design). These dual-speed stepper motors can operate at two different step sizes simultaneously using two racks.

In order to evaluate the motion time for the dual-speed stepper motors under ideal conditions i.e. inside the MRI environment, the operating frequency of the motors will be set at 10 Hz. While operating the robot manually, the exact positioning of the robot is quite difficult at the first attempt and requires multiple tries. As a result, a reverse technique will be used. The MATLAB kinematics script, which gives the number of steps every joint has to take, will be run for a series of random values along the X axis as per the robot coordinate frame (kinematically, for joints q1 and q2). For every step value of q1 and q2 obtained, the robot will be, initially, manually operated to the required position. Once the robot is at the desired position, the manual slider switches will be instantly dragged back all the way to zero. The time required for the robot to reach back to its starting position will be recorded. This operation can also be evaluated theoretically since the known frequency of operation is 10 Hz which translates to 10 steps per second. Thereafter, a comparison will be made between the theoretical evaluation and the practical evaluation results. As intended, a comparison will also be made between the operating times of the SUNRAM 5 and the Stormram 4 for the same input parameters.

Additionally, the positioning accuracy of the stepper motors has also been computed theoretically. Naturally, the positional accuracy depends on the step sizes that are achievable by the motors. Based on the step sizes of the dual-speed stepper motors, the positional accuracy that can be achieved is a multiple of 0.1mm. This means that theoretically, the dual-speed motors can reach every position that is a multiple of 0.1mm accurately. A set of random distances to be traveled by the dual-speed stepper motors will be taken for evaluation and the most accurately reachable distance value will be computed theoretically. This will then be compared to the theoretically most accurately reachable distance value for the Stormram 4 as well for comparative analysis.

4.4.2 Analysis of the Robot Movement Space & Workspace

Since the robot is intended to be used inside an MRI scanner, an analysis of the space required for the robot to operate will be performed. During every operation, it is essential that the robot will completely circumvent the grating. Therefore, before the start of any operation, the robot will be in its base position. The base position is defined such that the needle perfectly aligns with the radius of curvature of the base rack when the robot is near the extreme left end of the base rack. The SUNRAM 5 has six joints in total and the joint configuration vector q (q1-q6), which defines the number of steps that every joint has to take in order to reach the target. While calculating the total workspace volume, the breast fixation system has not been taken into account since it can be used to fix the breast of the patient. The base rack of the robot excluding the fixation system part is about 10cm wide. However, when the robot is in a pose where the needle is completely retracted, the actual body of the robot extends outside the width of the base rack. In order to compute the total movement space of the robot, the robot was moved in 4 different poses such that it was positioned at extremities both in the X and Y direction as per the robot coordinate frame. An overall movement space was computed based on the results.

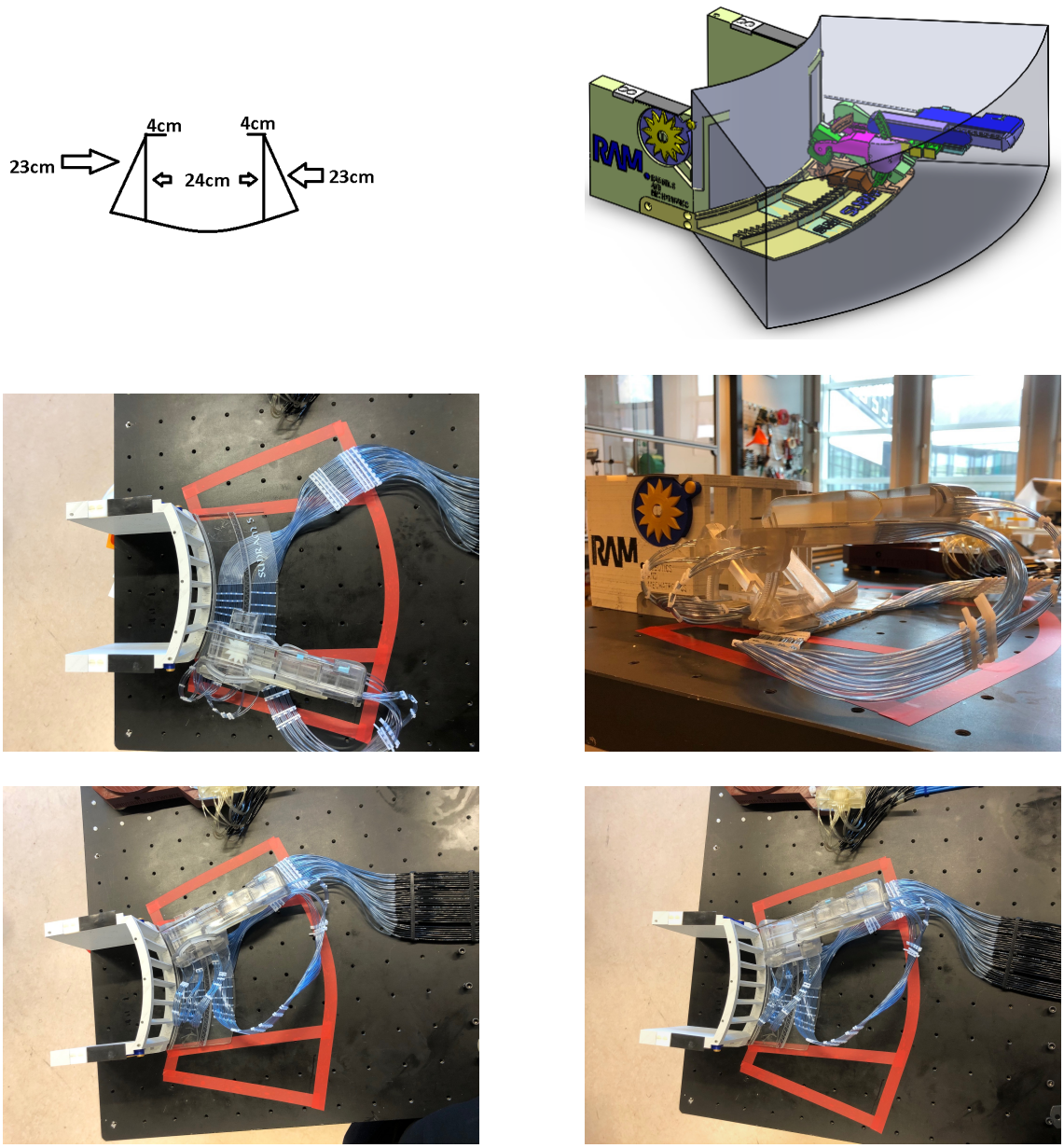

Figure 4.3: First Row: Left - Measured Dimensions of Robot Movement Space, Right - Graphic Illustration in Solidworks
Second Row: Left - Extreme left lowermost position, Right - Extreme left highermost position
Third Row: Left - Extreme right lowermost position, Right - Extreme right highermost position

The average diameter of a wide bore MRI scanner is about 70 cm (GE Healthcare). A study shows that in Sweden, the average shoulder to shoulder measurements for men is no more than 40 cm and that for females is no more than 36 cm (Healthline.com). The unique breast fixation system that is a part of the SUNRAM 5 allows the user to orient the approach of the robot towards the breast such that it can approach the breast from the side as well as from the chin side or waist side. Considering that the average shoulder to shoulder width of a Swedish man is about 40cm, it leaves about 15 cm space on either side of the person. Keeping in mind the fact that the breast to breast width of any person is lesser than the shoulder to shoulder width, the SUNRAM 5 should easily be able to operate inside the wide bore MRI scanner leaving

enough space on either side. Additionally, to approach from the side of the breast, the patient can be positioned offcenter inside the MRI scanner to make more room on the side where the robot needs to operate.

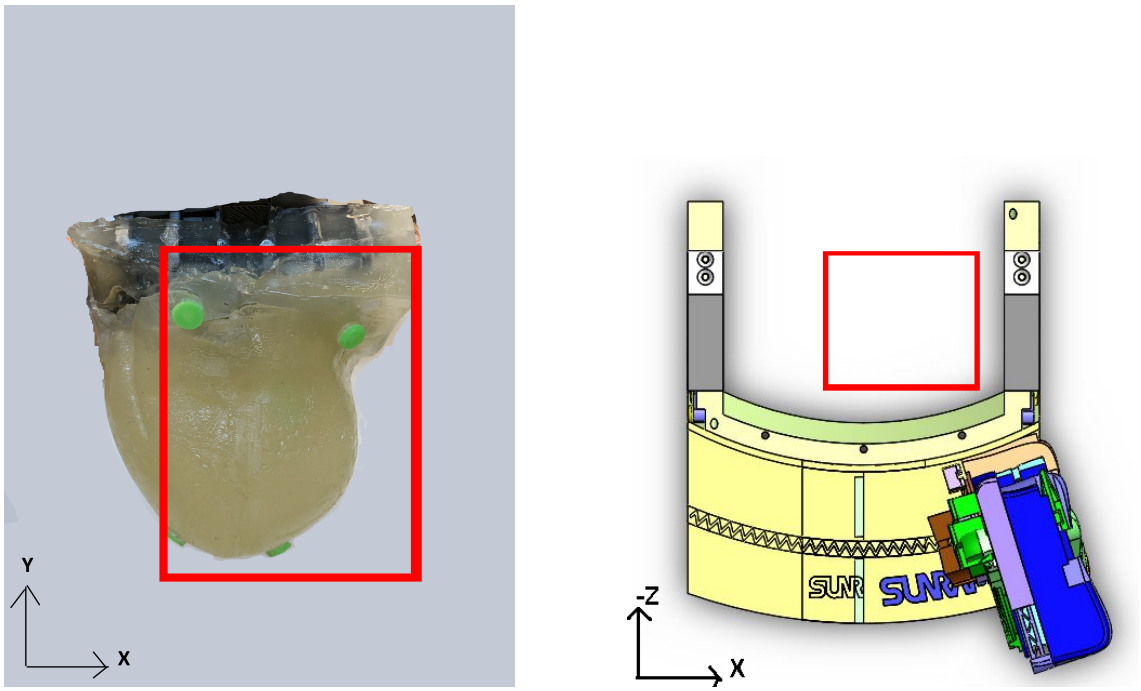

Figure 4.4: Left - Reachable Workspace of the Needle tip XY plane, Right - Reachable workspace of the Needle tip -ZX plane

In addition to the movement space required by the robot, the reachable workspace of the robot is also evaluated. The reachable space of the robot is the space that can be reached by the needle tip thus enabling the biopsy operation within that space. Like the moveable workspace of the robot body, a reachable workspace of the needle tip was also computed based on the kinematic configurations generated using the MATLAB script. The two non-operational motors of the SUNRAM 5 did not matter here since only the output from the kinematics script in MALTAB (Zwiep(2020)) was considered. The script was supplied with input values of target coordinates as per the robot coordinate system Figure 4.1. The range of the target coordinates given as the input to the MATLAB script varied from minimum to maximum of the possible values. The criteria was defined such that the needle tip should reach the point with an accuracy of more than 0.1mm.

	X (mm)	Y (mm)	Z (mm)
Minimum	72	0	-73
Maximum	163	108	-126

Table 4.2: Minimum and Maximum values of the target coordinates which the needle tip can reach with an accuracy of more than 0.1mm as per the output of the kinematic script

The coordinates have been defined in terms of the robot coordinate system Figure 4.1. There are still a few input coordinates for which the needle tip does not reach the target with an accuracy of more than 0.1mm, however the above mentioned range gives a fair estimate of the accurately reachable area of the SUNRAM 5 needle tip.

4.4.3 Evaluation of Accuracy - In Air measurements

Before the robot is operated in the MRI environment, in-air evaluation of the robot will be conducted without actually using a breast phantom. The positional accuracy tests in air will be performed by placing a sheet of paper at a known location in the -Z direction (Z=-75mm). The sheet of paper positioned will have 5 targets at random locations in the XY plane withing the workspace of the SUNRAM 5. This will provide us with sufficient idea about the targeting accuracy of the needle tip of the SUNRAM 5.

The target coordinates will be supplied to the MATLAB App in terms of the robot coordinate system Figure 4.1. The MATLAB script will calculate the corresponding coordinates in terms of the kinematic coordinate system Figure 4.1. These target coordinate locations will then be used and the kinematic equations will help in calculating a suitable joint configuration vector for the SUNRAM 5. The joint configuration vector in our case is a vector q(q1,q2,q3,q4,q5,q6) which specifies the number of steps every stepper motor has to take to reach the required target point. The Arduino controller is the main controller responsible for controlling the valves of the manifold thereby controlling the movement of the stepper motors. The manual sliders are operated to move the robot to by the desired number of steps. Once the Arduino receives this joint configuration vector, it selectively controls the valves to make the motors take the desired number of steps. Feedforward is the control method and there is no feedback from the system in terms of its current position.

The positional accuracy will be measured by measuring the offsets from the target position along the X and Y direction at the point of piercing in the paper. Once the entire sequence of 5 targets is complete, the sheet of paper will be replaced and the entire sequence will be repeated 2 more times in order to evaluate the standard deviation and check the repeatability of the system. The measurements will be done in MATLAB by taking a photograph of the evaluation sheet and measuring the distances using the 'imtool' command. The calibration between real life and image distances will be done by arbitrarily drawing 1 cm lines at 4 locations on the sheet as a known distance. Corresponding results are documented in the next chapter.

4.4.4 Evaluation of Accuracy - In MRI measurements

Once the evaluation of the robot in air is complete, the SUNRAM 5 is intended to be evaluated inside the MRI environment. The scanner used will be the Esaote G-scan Brio 0.25T scanner. It was not practically possible to take the robot to the MRI room because of certain restrictions, hence a workaround method will be used. The target is a cuboidal phantom. An almost transparent cuboidal phantom (800g Plastilleure Soft, 200g Assouplissant Plastilleure) embedded with green dye stained PVC plastisol lesions will be used. 3 target sites will be pre-defined inside the phantom. The error, of course, is defined as the distance between the defined target points and the reconstructed needle position. The SUNRAM 5 has a fixation system to immobilize the phantom from the rear side therefore the breast phantom itself will be immobilized. However, further deformations will not be taken into account. The motors ofcourse will be again operated at 10 Hz, the standard achievable frequency inside the MRI scanner with 5m long tubes. The idea is that the phantom along with the fixation system will all be positioned in a fixed place in the lab. This entire setup will then be carried to the MRI room and an MRI scan will be made. The MRI scanner itself will initially be calibrated using a custom 3D grid pattern. This is done in order to apply a geometric correction function however it only needs to be done once. Once the MRI scan is available, the entire setup will be brought back to the lab. Although the measurements will be done outside the MRI scanner, the target locations will be chosen from the MRI scan itself. This will be the same as an actual MRI based evaluation except for the fact that it will be performed in the lab.

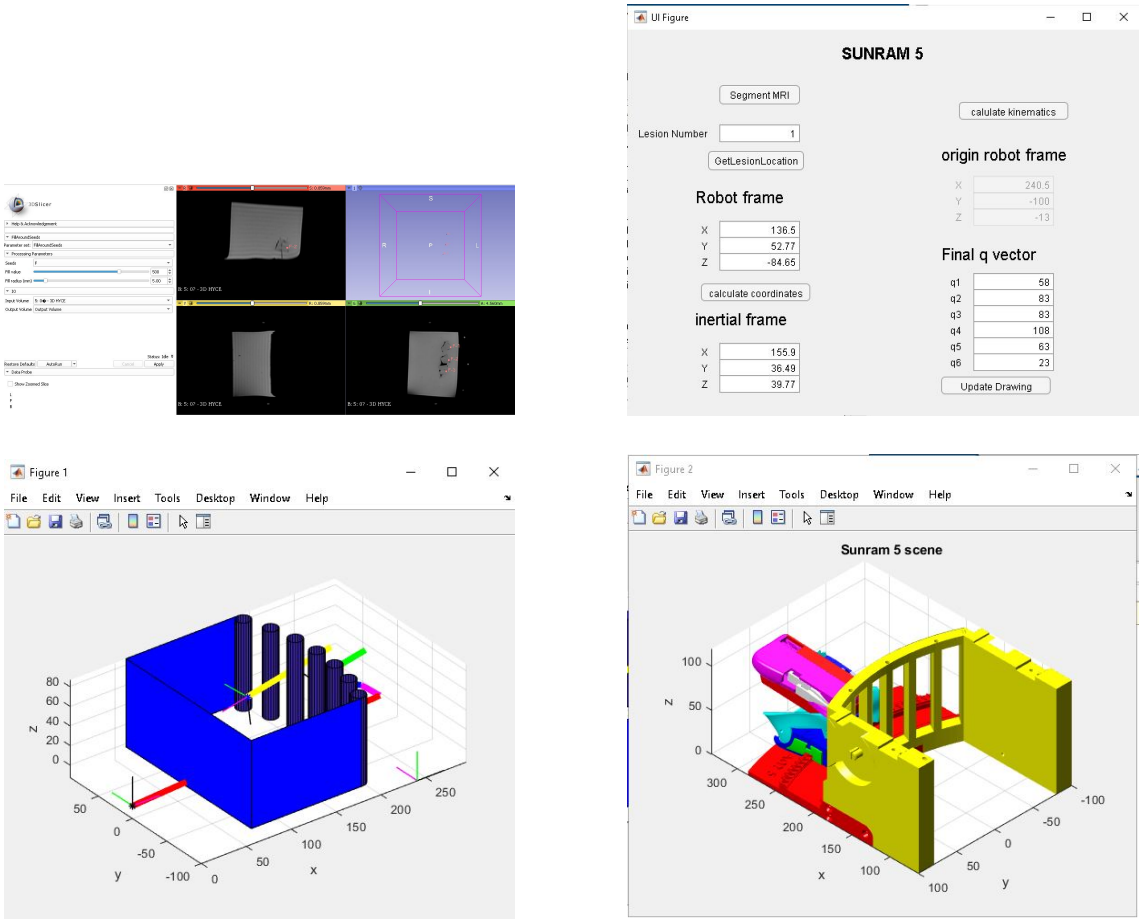

Figure 4.5: Left top - 3D slicer interface for target selection using customized MATLAB module, Right top - MATLAB 'MRIprocessapp' interface for segmenting MRI, selecting lesion and calculating kinematics, Left bottom - Skeleton frame drawing showing location of needle tip, Right bottom - Graphic rendering of the robot in final pose

A detailed description of the evaluation procedure is as follows -

1. Initially, the fixed setup is brought into the MRI room and a pre-operative scan using the fixation system as well as the phantom is performed in order to segment the markers and define the robot coordinate system Figure 4.1.

2. Next, the available MRI scan is viewed in the 3D slicer software. The 3D slicer software provides the ability to volume render an MRI scan and for the doctors to drop target markers at desired target locations. The doctors also have the functionality to select more than 1 target at a time. On completing the operation, the coordinates of all these markers will be directly sent to MATLAB Figure 4.5 left top.

3. Once the coordinates are available in MATLAB, the next step is to operate the 'MRIprocessapp'. On starting the app, the first step is to press the 'Segment MRI' button which will segment the MRI scan to get the transformation matrix. Additionally, the app interface provides the ability to choose which target the robot should target next. The target number is the same as the dropped fiducial number Figure 4.5 right top.

4. Once the target is selected, pressing the 'Get Lesion Location' key on the app will get the coordinates of the target in terms of the robot coordinate system Figure 4.1. These coordinates can then be further used to calculate the target coordinates in terms of the

kinematic coordinate system Figure 4.1 by pressing the 'Calculate Coordinates' key. This is then followed by pressing the 'Calculate Kinematics' key to obtain the joint steps configuration vector Figure 4.5 left bottom. The 'Update Drawing' key will show a graphic rendering of the robot Figure 4.5 right bottom.

5. The 'Calculate Kinematics' key will give the number of steps that every motor has to take in order to reach the desired end configuration. The robot is then manually operated to take the desired number of steps using the sliders on the controller box.

6. Once the needle movement is complete, the system is photographed from the top and front in order to confirm the lateral location of the needle. The measurements are done using the 'imtool' command in MATLAB.

7. Once the location of the needle tip is confirmed, the switch on the controller box can be used to fire the biopsy gun and a sample can be acquired.

8. In case where there are more than one targets, the motors q5 and q6 can be completely retracted in order to extract the sample from the biopsy gun. Once the sample has been extracted, a new target number can be selected and the procedure can be repeated from step 4 onwards until all targets are covered.

For every target, the error between the target point and the needle tip will be computed using front and top view photographs taken using a phone camera (Apple iPhone 8+). These will then be analyzed using the MATLAB function 'imtool' to find the errors in the X and Y direction as per the robot coordinate system Figure 4.1. The experimental procedure has been developed taking into consideration the actual clinical MRI based breast biopsy procedure. Detailed results will be documented in the next chapter.

After completing this part, an attempt will be made to estimate the effect of the breast fixation system. The breast fixation system is one of the key additions to the SUNRAM 5 from its predecessor. The breast fixation system was introduced in order to minimize the movement of the phantom thereby trying to reduce the effect of the interaction between the needle and the phantom.

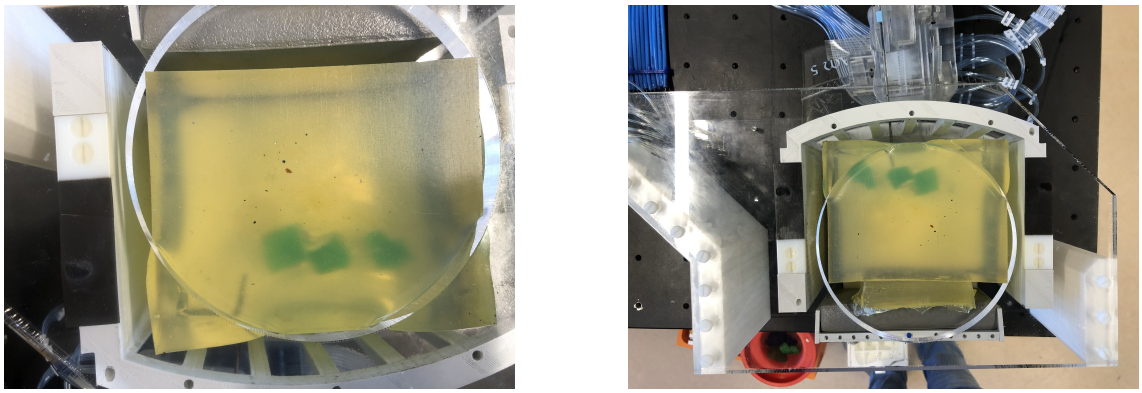

Figure 4.6: Left - Experimental setup with a gap between the phantom and the rear support, Right - Dummy filler inserted to remove gap between rear support and phantom to induce effect of the breast fixation system

During the initial MRI based evaluation procedure, the breast fixation system was not implemented. There was a gap between the phantom and the rear support of the breast fixation system thereby allowing the phantom to freely move in the X and Z direction as per the robot

coordinate system Figure 4.1. However, after the first set of experiments, the gap was filled with a filler material inserted which is same as the material of the phantom. This was done in order to induce the effect of the breast fixation system. This would ideally minimize the movement of the phantom in the Z direction thereby minimizing the effect due to the needle tissue interaction. An evaluation was done with this updated setup in place by measuring positioning errors for the same targets as before. Detailed results are documented in the next chapter.

4.4.5 Evaluation of Quality of Biopsy Samples

The SUNRAM 5 has been equipped with a fireable biopsy gun. This biopsy gun is similar to a real biopsy gun thereby giving the robot the capability to extract a tissue sample similar to an actual biopsy procedure. A small evaluation will be done to assess the quality of the biopsy samples taken. A test will be classified as a successful biopsy if the sample is at least 15mm in length as is the case in a standard biopsy procedure. Results will be documented in the next chapter.

4.4.6 Full Clinical Biopsy Procedure Evaluation

The SUNRAM 5 has a unique breast fixation system that allows the breast biopsy procedure to be completed in the prone position. In addition to that, the SUNRAM 5 is MR safe (apart from the standard MR compatible biopsy needle) and compact enough to be placed inside an MRI scanner, and also has the ability to fire a biopsy gun to collect biopsy samples. Therefore, the SUNRAM 5 has the potential to perform a full clinical breast biopsy procedure inside an MRI environment.

A full clinical biopsy procedure is explained earlier. Correspondingly, the SUNRAM 5 will also be evaluated while performing a full clinical biopsy procedure. The patient of course has been replaced by a phantom and the pre-operative medical procedures such as giving the patient injections, IV drip, and contrast agent are not a part of the SUNRAM 5 workflow and are considered to be done before the procedure. A full clinical biopsy procedure from the point of view of the SUNRAM 5 is as follows -

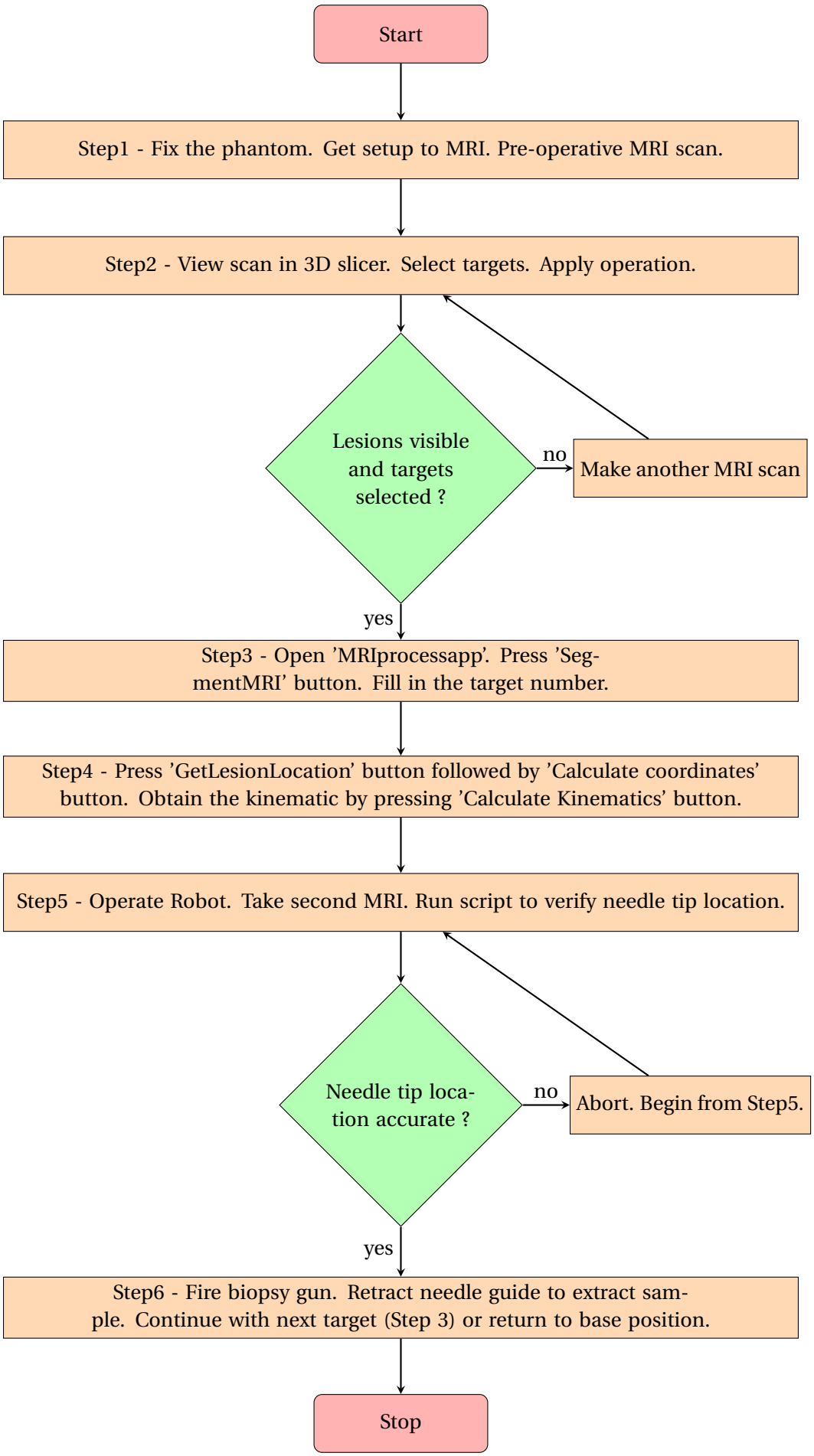
Start
Step1 - Fix the phantom. Get setup to MRI. Pre-operative MRI scan.
Step2 - View scan in 3D slicer. Select targets. Apply operation.
Lesions visible and targets selected ?
no
Make another MRI scan
yes
Step3 - Open 'MRIprocessapp'. Press 'SegmentMRI' button. Fill in the target number.
Step4 - Press 'GetLesionLocation' button followed by 'Calculate coordinates' button. Obtain the kinematic by pressing 'Calculate Kinematics' button.
Step5 - Operate Robot. Take second MRI. Run script to verify needle tip location.
Needle tip location accurate ?
no
Abort. Begin from Step5.
yes
Step6 - Fire biopsy gun. Retract needle guide to extract sample. Continue with next target (Step 3) or return to base position.
Stop

- Step 1 - Initially, the phantom is fixed with the SUNRAM 5 breast fixation system and the whole setup is brought inside the MRI room. A pre-operative scan is performed in order to identify the markers and localize the lesion.
- Step 2 - Next, the available MRI scan is viewed in the 3D slicer software. The 3D slicer software provides the ability to volume render an MRI scan and for the doctors to drop target markers at desired target locations. The doctors also have the functionality to select more than 1 target at a time. Upon completing the operation, the coordinates of all these markers will be directly sent to MATLAB.
- Step 3 - Once the coordinates are available in MATLAB, the next step is to operate the 'MRIprocessapp'. On starting the app, the first step is to press the 'Segment MRI' button which will segment MRI scan to get the transformation matrix. Additionally, the app interface provides the ability to choose which target the robot should target next. The target number is the same as the dropped fiducial number.
- Step 4 - Once the target is selected, pressing the 'Get Lesion Location' key on the app will get the coordinates of the target in terms of the robot coordinate system Figure 4.1. These coordinates can then be further used to calculate the target coordinates in terms of the kinematic coordinate system Figure 4.1 by pressing the 'Calculate Coordinates' key. This is then followed by pressing the 'Calculate Kinematics' key to obtain the joint steps configuration vector. The 'Update Drawing' key will show a graphic rendering of the robot.
- Step 5 - The 'Calculate Kinematics' key will give the number of steps that every motor has to take in order to reach the desired end configuration. The robot is then manually operated to take the desired number of steps using the sliders on the controller box. Once the robot has reached the position based on the number of steps traveled, another MRI scan will be performed to confirm the location of the needle tip. An automatic script (same as the one used in Stormram 4) will be used to segment the needle locations.
- Step 6 - Once the location of the needle is confirmed, and correct, the biopsy gun will be fired and the sample collected. The biopsy operation is now complete. The needle guide of the robot will be retracted to its extreme position and the sample will be collected. Simultaneously, the 'MRIprocessapp' can be used to compute the robot kinematics for targeting the next lesion.

The full biopsy procedure using the SUNRAM 5 involves multiple steps like an actual biopsy procedure. However, most of the time in an actual biopsy procedure is taken up by the MRI scanner in taking the scans. That is also the case in the SUNRAM 5 based biopsy. However, time taken for performing an MRI scan is hugely dependant on multiple factors such as the strength of the MRI scanner and visibility of the lesion based on its location. Therefore, a time taken for a scan is always relative and hence, a fair comparison is only possible by not considering the time taken per MRI scan. However, the fundamental differences in timings between the two procedures will be evaluated taking into account the tasks that are not required to be performed using the SUNRAM 5 when compared to a standard MRI guided breast biopsy procedure.

5 Experimental Results and Discussion

This section documents the detailed results of the evaluation of the various aspects of the SUNRAM 5. The evaluation of the SUNRAM 5 robot was done to evaluate the performance of certain individual components of the robot and to test its ability to perform a full clinical biopsy procedure.

5.1 Dual-speed Stepper Motors Evaluation

Since the SUNRAM 5 has been implemented with dual-speed stepper motors, the system can move with multiple step sizes simultaneously thereby being able to cover a larger distance in lesser time. An evaluation was performed in order to theoretically assess the positional accuracy of the dual-speed stepper motors and experimentally measure the procedure time required.

In the SUNRAM 5, for the dual-speed stepper motors, the step sizes are 1.7mm and 0.3mm. This means that the dual-speed motors can theoretically reach every distance accurately which is a multiple of 0.1mm. The Stormram 4 on the other hand only has a single-speed motor with a step size of 0.25mm and thus only capable of reaching a point that is at a distance equal to the multiples of 0.25mm. The table below shows the closest accurately achievable distance by both the robots. The distances chosen have been chosen arbitrarily with a resolution of up to 2 decimal places.

Distance along X axis (mm)	SUNRAM 5 - Closest Achievable Distance (mm)	Stormram 4 - Closest Achievable Distance (mm)	Improvement in positioning accuracy by the SUNRAM 5 (mm)
0.1	0.1	0	0.1
0.85	0.8	0.75	0.05
1.7	1.7	1.75	0.05
4.35	4.3	4.25	0.1
30.6	30.6	30.5	0.1
79.8	79.8	79.75	0.05

Table 5.1: Theoretical Positioning Accuracy of the SUNRAM 5 and Stormram 4 showing that the SUNRAM 5 can be at most 0.1mm more accurate than the Stormram 4 in the given direction

As can be seen from the table, theoretically, the SUNRAM 5 can reach every point which is multiple of 0.1mm in the direction of motion of the dual-speed stepper motors. As opposed to this, the Stormram 4 could theoretically only reach a target point in multiples of 0.25mm. A practical evaluation could not be conducted since both the smaller step size motors which were of the dual-speed motors were not functioning. By looking at this table, we understand that since the SUNRAM 5 uses dual-speed stepper motors for movement in the X and Z direction as per the robot coordinate system Figure 4.1, it can be by at most 0.1mm closer to the target as compared to the Stormram 4.

However, a practical evaluation has been done for evaluating the operating time required for the motors to reach a certain distance (distances in the robot coordinate frame). The experiment was performed with all the motors operating at a frequency of 10 Hz which is the ideal frequency achievable inside an MRI room when the robot is being operated using 5m long tubes. A theoretical calculation of the motion time has also been presented along with the

results of an experimental evaluation. A comparison has been made between the theoretically calculated motion time and the experimentally measured motion time. The Stormram 4 was then also operated to the same distance as traveled by the SUNRAM 5 and a comparison will be made between the two.

Distance X (mm)	Motor steps (q1, q2)	Motion Time (Ideal) (sec)	Motion Time (Measured) (sec)	Motion Time (Video) (sec)	Physical Measurement Error (sec)
94	30, 24	3.00	3.32 ± 0.08	3.13 ± 0.06	0.19 ± 0.14
108	7, 129	12.90	13.15 ± 0.14	13.03 ± 0.03	0.15 ± 0.14
131	63, 60	6.30	6.65 ± 0.03	6.40 ± 0.03	0.25 ± 0.06
145	91, 29	9.10	9.41 ± 0.07	9.13 ± 0.09	0.28 ± 0.16
158	80, 102	10.20	10.41 ± 0.13	10.30 ± 0.06	0.17 ± 0.13

Table 5.2: SUNRAM 5 ideal, measured and video analysed motion time for movement along X direction showing that video analysis gives a better measurement, the SUNRAM 5 measured motion times and ideal times are within physical measurement error

The table above gives shows the ideal and measured motion time for movement along X direction using the dual-speed stepper motors. The ideal time is calculated based on the stepping frequency which is 10 Hz i.e. 10 steps per second. The measured motion time was measured on the Apple iPhone 8+ stopwatch. The difference between the ideal and measured motion times is due to the physical errors during measurement such as the delays in starting and stopping the stopwatch as well as due to the internal noise in the electronic and pneumatic circuit. Additional delay is also introduced due idle time from the Arduino since the Arduino has been programmed to wait until it receives a stable value from the slider ADC's before it controls the valves. The standard deviation in the measured difference is due to the physical measurement delay.

In order to eliminate the difference due to the physical measurement errors and due to the idle time of the Arduino, measurements were done by doing a frame by frame analysis of a video of the controller display to measure the absolute movement time required for the robot. The table shows a comparison between the measured motion time and the absolute motion time found out via the frame by frame analysis of the video. The absolute motion times are closer to the ideal timings. The difference between the measured motion times and the motion time computed from the video analysis is termed as the physical measurement error. It includes the physical error while measuring (such as pressing the start and stop button of the stopwatch) as well as the idle time of the Arduino before it starts to control the valves. The motion time extracted from the video is the absolute motion time that the dual-speed stepper motors require to operate. The difference between the video time and ideal time can be attributed to internal delay of the ADC, Arduino and other circuitry, switching delay from the valves (switching time of valves is 2 ms) and delay in the pneumatic tubes and pump, and due to the frame rate delay in the camera used to record a video.

In order to perform a comparative study, the same measurements were repeated with the Stormram 4 which has a single-speed stepper motor with a step size of 0.25mm. The Stormram 4 was also made to move the same distance at a stepping frequency of 10 Hz.

Distance X (mm)	Motion Time Stormram 4 (Ideal) (sec)	Motion Time Stormram 4 (Measured) (sec)	Motion Time SUNRAM 5 (Measured) (sec)	Ratio of Motion Times (SUNRAM 5 / Stormram 4)
94	11.60	11.55 ± 0.17	3.32 ± 0.08	3.48
108	17.20	16.71 ± 0.21	13.15 ± 0.14	1.27
131	26.40	25.02 ± 0.06	6.65 ± 0.03	3.76
145	32.00	31.35 ± 0.11	9.41 ± 0.07	3.33
158	37.20	36.32 ± 0.12	10.41 ± 0.13	3.49

Table 5.3: Comparison between SUNRAM 5 and Stormram 4 motion times showing that the SUNRAM 5 is on an average upto 3.07 times faster

The table shows the measured motion times for the Stormram 4 which are always close to the ideal times however never more. In general, the SUNRAM 5 is always faster than the Stormram 4 while moving in the axis of motion which uses the dual-speed stepper motors. The factor by which the SUNRAM 5 is faster is dependant more on the number of steps taken by the robot rather than the distance to be traveled. As can be seen in the case of X=108mm, the SUNRAM needs to take comparatively more number of maximum steps (129) and as such the factor by which the SUNRAM 5 is faster, reduces. Additionally, the factor of 'fastness' has errors due to physical measurement errors which have not been accounted for.

The achieved frequency was also computed using the ideal and observed motion times. Additionally, the difference between the analyzed motion time from the video and the ideal time as per mathematical calculations has been plotted.

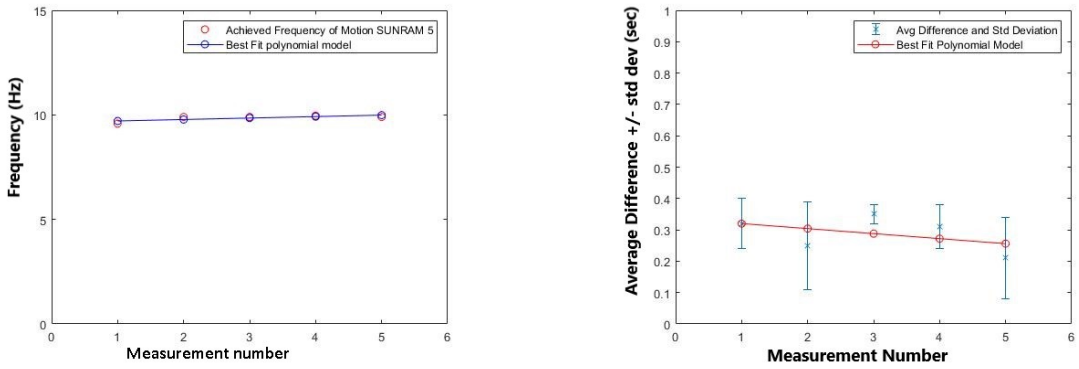

Figure 5.1: Left - Graph showing achieved almost constant frequency with a best-fit polynomial indicating that SUNRAM 5 rightly operates at the set frequency of 10 Hz, Right - Differences between ideal and stopwatch measured motion times and a best-fit polynomial line indicating that the measured time will on an avg lag by about 0.3 sec due to physical and internal errors

The frequency achieved in all measurements was almost close to 10 Hz. The loss in frequency was again due to the delay factors in the circuit. An almost constant difference between the video analyzed and ideal motion times also suggests that the error was almost constant and coming from the same internal sources from the hardware.

5.2 Needle Tip Accuracy measurements - in Air

The positional accuracy of the SUNRAM 5 was evaluated in air using sheets of paper with 5 targets on every sheet. The sheet of paper was positioned at -75mm position along the -Z axis. The reason why only 5 targets were chosen and only placed at one position along the -Z axis is

that two of the small step stepper motors part of the two dual-speed stepper motors (named as motor q2 and q5 in the kinematic configuration) were non-functional due to physical damage. It was practically not viable to reprint the parts again and hence the positions and the targets were compensated such that the targets were reachable with maximum accuracy. When the targets were fed in the MATLAB script, a vector with the steps to be taken for each motor was obtained. Since motor q5 and q6 operate along the same axis, the motion of q5 could always be compensated using q6 and the step number was rounded up to the nearest integer value. However, motors q2 and q1 do not move in the same axis and hence it was not possible to compensate the motion of q2 using q1. Hence, motor q2 did not take any steps and the error arising due to that was considered before as the expected offset between achievable position and actual target position. Additionally, based on the output from the MATLAB script in terms of the skeleton model, the expected needle tip position was also available. The difference between the expected needle tip position and the desired needle tip position was also added to the expected offset. Having defined the targets and expected offsets, the robot was individually made to move towards the targets and consequently the X and Y offsets of each puncture relative to the target were measured. These were compared with the expected offsets and the absolute positioning error in targeting accuracy was found out as the difference between the expected offset and the measured offset. The entire experiment was repeated 3 times to test the repeatability of the system. All the positions and errors have been expressed in the kinematic coordinate system Figure 4.1.

No. of sites targeted - 5 on one sheet x 3 times									
Target	Target Position (mm)			Expected Offset (mm)			Positioning Error (mm)		
	X	Y	Z	X	Y	Z	$\mu_x \pm \sigma_x$	$\mu_y \pm \sigma_y$	$\mu_z \pm \sigma_z$
1	165.53	-12.00	45.00	-0.27	-7.19	0.02	0.24±0.04	0.30±0.29	0.18±0.03
2	165.53	28.00	55.00	-0.75	-0.42	0.02	0.20±0.10	-0.20±0.30	-0.26±0.53
3	165.53	8.00	40.00	-0.02	-1.19	0.00	0.18±0.05	0.32±0.32	-0.34±0.20
4	165.53	28.00	43.00	-1.15	-0.42	0.02	0.24±0.04	-0.32±0.19	-0.25±0.44
5	165.53	5.00	48.00	-0.27	-0.36	0.01	0.23±0.02	-0.72±0.45	-0.11±0.16

Table 5.4: Accuracy of Needle Tip placement along with deviations between three readings showing sub millimeter needle tip positioning error

For every repetition, the positioning error, which is the difference between expected offset and measured offset, and the standard deviations were calculated for all 5 measured points in the X and Y axis. As can be observed from the table, all the errors are within sub-millimeter accuracy. The errors have been measured according to any standard coordinate system where error to the right of the target is positive and to the left is negative. Apart from 1 set of readings, the SUNRAM needle tip has a tendency to steer biased in the left and bottom directions of any target point. Based on the readings, the SUNRAM 5 achieved a needle tip placement accuracy of 0.68mm in the Y direction and 0.5mm in the Z direction as per the kinematic coordinate system Figure 4.1. Based on the width of the puncture holes, the accuracy in the X direction as per the kinematic coordinate system was estimated to be around 0.27mm.

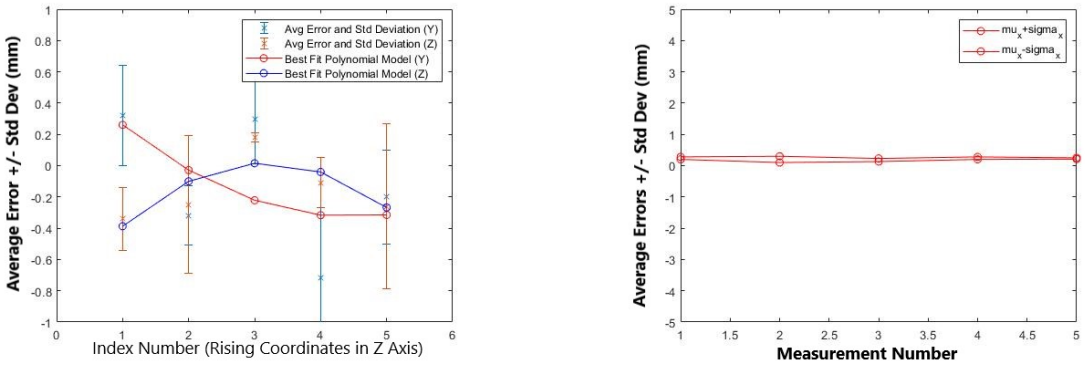

Figure 5.2: Left - Error range with deviations and best fit models showing no relation between error and position in Y and Z direction, Right - Graph showing almost constant errors as expected in X direction

In the graph on the left, the targets have been plotted in increasing order of target coordinates in the Z axis. The graph on the left shows that the range of errors is always in the range of -1 to 1 in the Y and Z axis. This would mean that these errors are not fundamental positioning errors but rather constant errors introduced either due to the kinematic incapability of the design or due to the inaccurate positioning of the evaluation sheet and fixation system. Additionally, the almost fixed height of the error bars also shows that the deviation between 3 sets of measurements was constant for all 5 targets most likely due to differences in distance calibration while measurement in MATLAB or the inaccuracies in sheet positioning. Using a small evaluation, it was estimated that the average sheet positioning error is about 0.56mm in the Y axis and 0.495mm in the Z axis. If these errors are subtracted from the measured positioning errors, the actual positioning error would be about 0.12mm in the Y axis and 0.005mm in the Z axis. To further evaluate, a best fit 2^{nd} order polynomial model was made to fit the points. It was observed that the positioning error is independent of the target values of Y and Z. There is no observed relation between an increase in Z values and the mean positioning errors. Additionally, manual errors while performing the measurements using the MATLAB 'imtool' function have not been taken into account. Also since the position of the paper sheet was at a constant position along the X axis, the errors in the X axis were also expected to be constant. The graph on the right shows that the errors along the X axis are almost constant.

Numerous other observations were also made while performing the experiments. There was a sag in the robot in the rear tail end of the robot due to the weight of the rear part itself. However, at its base position, the needle of the robot needs to be in parallel with the XY plane as per the kinematic coordinate system Figure 4.1. Therefore, in order to compensate for this, a systematic offset of exactly 8 steps was required in motor q4. This offset was already taken into account before doing the measurements. Additionally, switching off the robot mid-operation displaces motor q3 since it is not able to hold its position without the application of pneumatic pressure. Motor q6 needs to be aligned properly in its base configuration based on the transformation matrix defined between the needle tip location and the robot. This is marked by a black marker on the robot body and accurate needle positioning is only possible in the Z direction (robot coordinate frame) when q6 starts in the right position.

5.3 Needle Tip Accuracy Measurements - MRI

Once the evaluation of the system was complete with paper sheets, further evaluation was intended to be done with a phantom in place based on an MRI scan. In order to evaluate a full clinical procedure, it was important to initially test the accuracy of the needle tip placement

in a phantom based on positions from a segmented MRI scan. As discussed in the experiment section above, a cuboidal phantom (800g Plastilleure Soft, 200g Assouplissant Plastilleure) was used for this purpose. The MRI scan was performed using the Esaote G-scan Brio 0.25T scanner. The MRI scan was segmented to locate the lesions (targets) as well as for registration of the markers in order to define a coordinate transformation. Once the coordinates of the targets were available in terms of the robot coordinate frame, the MATLAB script was used to find the joint configuration vector giving the number of steps every motor has to take. The robot was manually operated to the location and measurements were done using photographs taken from a phone camera (Apple iPhone 8+). This time again, motors q2 and q5 were not functioning. The motion of q5 can be compensated using q6 since they move along the same axis. However, q6 can only move 35 steps and as such any further steps were considered as an expected offset. Since q2 and q1 do not move along the same axis, the steps that q2 was not able to take were considered as an expected offset. The positioning error has been defined here as the difference between the expected offset and the measured offset from the photographs. All distances and positions are mentioned in the robot coordinate system Figure 4.1.

No. of sites targeted - 3 x 3 times								
Target	Target Position (mm)			Expected Offset (mm)			Positioning Error (mm)	
	X	Y	Z	X	Y	Z	$\mu_x \pm \sigma_x$	$\mu_y \pm \sigma_y$
1	136.49	52.77	-84.65	-24.90	0.01	0.01	-2.05 ± 0.82	5.59 ± 0.27
2	90.44	59.13	-86.35	-6.30	0.02	-3.40	0.14 ± 1.67	2.76 ± 0.15
3	110.51	60.40	-81.68	0.00	0.01	0.02	0.73 ± 1.01	NA

Table 5.5: Accuracy of Needle Tip placement showing dependancy in error values based on the increase in Y coordinates

The table shows the positioning error which is the difference between the expected and the measured offset in positioning the needle tip. In case of an MRI based biopsy procedure, the lateral accuracy i.e. in our case the positioning accuracy in the X and Y direction as per the robot coordinate system Figure 4.1 is far more important than the accuracy in the direction of insertion. This is important because the biopsy needle is quite narrow and as such it needs to target the lesion area accurately to avoid missing. The biopsy gun, when fired, is fired in the direction of insertion and usually gets a sample of length 15-20mm. As a result, the accuracy in the direction of insertion is comparatively less important. As can be seen from the table, the errors are in range of millimeters. One thing that can be clearly spotted from the table is the fact that the error values have a clear dependency on the target coordinates in the Y axis. As the target Y value increases, the error in the needle tip position starts shifting from the left of the target towards the right direction. Additionally, the error in the Y direction starts decreasing in magnitude as the target Y value increases. As a general observation, the error in the Y direction is in general greater in magnitude than that in the X direction. Therefore, another observation that can be made is that the lack of the breast fixation pushes the needle upward due to the interaction between the needle and the phantom. The errors in the X and Y direction are most likely also influenced due to the inaccuracies in measurement in MATLAB in addition to those induced due to the needle phantom interaction. Additional error could have also been introduced due to physical movements in the phantom positions while moving the whole experimental setup from the lab to the MRI and back. Estimated error due to measurements in MATLAB and physical movement in the setup is about 1.2 mm. Taking the estimated errors into account, the average maximum error reduces to about 0.94 mm in the X direction and about 3.19 mm in the Y direction.

5.4 Breast Fixation System

The breast fixation system is one of the key additions to the SUNRAM 5 from its predecessor. The breast fixation system was introduced in order to minimize the movement of the phantom thereby trying to reduce the effect of the interaction between the needle and the phantom. While the initial evaluation was being done based on the MRI scan, the system was not equipped with the breast fixation system. As shown in Figure 4.6, the system was updated with a filler block to induce the effect of the breast fixation system. The entire experiment was performed exactly identical to the MRI based experiment performed earlier except this time with the effect of the fixation system in place.

No. of sites targeted - 3 x 3 times								
Target	Target Position (mm)			Expected Offset (mm)			Positioning Error (mm)	
	X	Y	Z	X	Y	Z	$\mu_x \pm \sigma_x$	$\mu_y \pm \sigma_y$
1	136.49	52.77	-84.65	-24.90	0.01	0.01	1.21 ± 0.41	3.86 ± 1.18
2	90.44	59.13	-86.35	-6.30	0.02	-3.40	2.30 ± 0.96	3.01 ± 1.40
3	110.51	60.40	-81.68	0.00	0.01	0.02	NA	NA

Table 5.6: Accuracy of Needle Tip placement with the fixation system showing comparatively lower errors in Y direction and increasing right-sided errors in X direction

The table shows the positioning error which is the difference between the expected and the measured offset in positioning the needle tip. As mentioned before, the positioning accuracy in the X and Y direction as per the robot coordinate system Figure 4.1 is far more important than the accuracy in the direction of insertion. As per the value shown in the table, the errors are in the range of millimeters. Like in the case of the MRI based experiments without the breast fixation system, the error values again have a clear dependency in Y direction with an increase in target Y value. The error values reduce as the target Y value increases which means that the robot clearly has kinematic problems in targeting values below 50mm in Y direction. Additionally, the angle at which the needle is inserted could also lead to higher errors in Y for certain target values because of the tendency to be deflected upward due to interaction between the needle and the phantom (where steps for q4 are less than q3). Additionally, dependency is observed between the errors in X direction and target values in Y. The error in the needle tip position starts on the right side of the target and keeps shifting more towards the right of the target as the target values in Y increase. This is most likely due to the effect of the breast fixation system and a manufacturing defect in the vertical rear lifter motor q4 causing it to tilt slightly. After the implementation of the breast fixation system, the error starts itself on the right of the target and continues to shift towards the right. Since the fixation system does not allow the movement of the phantom in the direction of insertion, the phantom tends to deform sideways leading to rising errors in X direction. The errors in the X and Y direction are most likely also influenced due to the inaccuracies in measurement in MATLAB in addition to those induced due to the needle phantom interaction. Additional error could have also been introduced due to physical movements in the phantom positions while moving the whole experimental setup from the lab to the MRI and back. The estimated error due to measurements in MATLAB and physical movement in the setup is about 1.2 mm. Taking the estimated errors into account, the average maximum error reduces to about 1.24 mm in the X direction and about 3.52 mm in the Y direction.

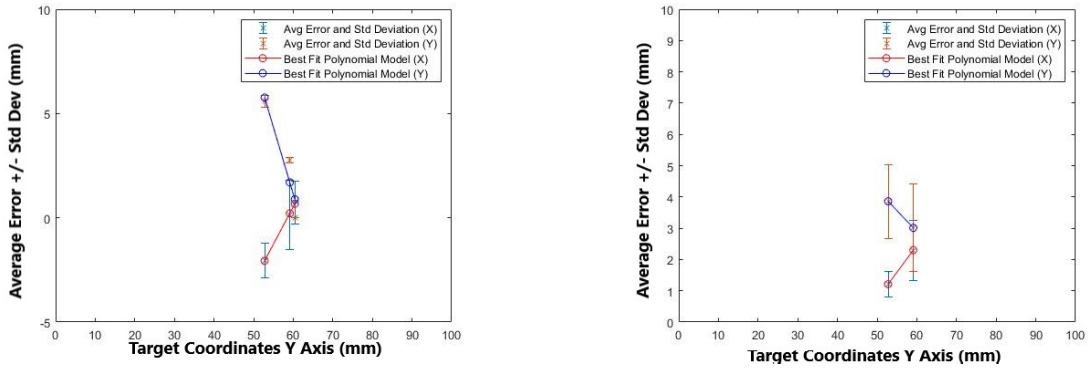

Figure 5.3: Left - Errors with deviations and best fit models showing relation between errors in X and Y direction and target positions along Y axis, Right - Graph showing same relation pattern between errors in X and Y axis and positions along Y axis with the breast fixation system as well

Both the graphs on the left and right show a clear dependency between the positioning errors in X and Y direction with respect to the target positions along the Y axis. As the target positions shift upwards along the Y axis, the errors in the Y axis reduce and those in the X axis start shifting from the left of the target in the right direction. Another unique thing that is observed with the use of the breast fixation system is that the errors in the Y direction are more or less in the same range as those without using the breast fixation system. However, with the use of the breast fixation system, the errors in the X are already on the right side of the target and keep shifting towards the right. This shows that the breast fixation system restricts deflection of the phantom in the direction of insertion thus causing it to deflect more towards the sides due to needle phantom interactions. As a result, the needle gets deflected more towards the right side.

5.5 Biopsy Samples

The SUNRAM 5 has been equipped with a unique biopsy gun firing mechanism. The biopsy gun can be fired thus enabling the SUNRAM 5 to take biopsy samples. In a standard commercial biopsy gun, the length of the sample that can be taken is about 15-20mm. The SUNRAM 5 biopsy gun is also capable of taking samples of around 15-20mm based on its design. A biopsy can be classified as successful if the size of the lesion in the sample is more than 3mm. The operating pressure was set at 2 bar while firing the needle. However, in this case, since 2 motors of the SUNRAM 5 were non operational, the needle was almost never able to reach the target. Therefore, on firing the biopsy gun, the sample so acquired was never expected to contain a part of the lesion. In this particular case, the biopsy operation was classified successful if the total size of the biopsy sample extracted is as per the standard biopsy sample size.

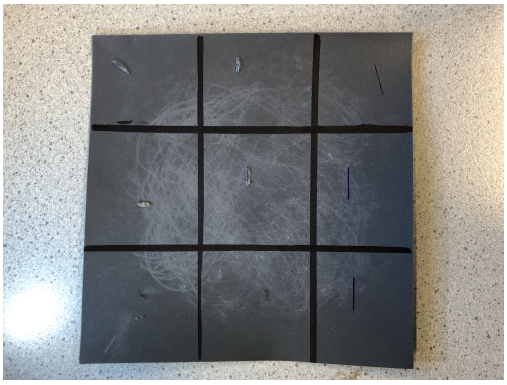

Figure 5.4: Biopsy samples of the phantom extracted where the coloums denote the target number

The length of the extracted sample was measured using the MATLAB 'imtool' function and was calibrated using 1 cm lines drawn on the sheet of paper. No samples were possible for target 3 (same as the targets used in the earlier experiments) since the non operational motors caused the needle to end up in front of the frame grating.

Biopsy Samples Extracted - 3 per target		
Target 1	Target 2	Target 3
6.89	4.84	NA
5.10	6.25	NA
3.11	3.17	NA

Table 5.7: Size of the biopsy samples extracted which are comparatively smaller than the size of a standard biopsy sample

The table shows the sizes of the biopsy samples extracted. Since all of the targets were consecutively targetted, the consecutive samples were bound to be ideally smaller than the first ones since the collection of one sample causes a gap in the phantom at the place of collection. Since the SUNRAM 5 is accurate within millimeters, the needle collects the sample from more or less the same place in the next iteration. In general, it can be clearly observed that the biopsy gun on the SUNRAM 5 was not able to collect samples like a standard biopsy gun. The size of the samples is comparatively smaller which could be due to a number of reasons. The design of the biopsy gun can be an important reason along with the force with which the biopsy gun was fired. The material and the stiffness of the phantom also plays an important part in the size of the samples acquired.

5.6 Full clinical procedure for MRI based biopsy

A SUNRAM 5 based full biopsy procedure was conducted as per the workflow given in the earlier chapter. Unfortunately, due to certain restrictions, the MRI scanner was only available for use once and as such could only be used for making a pre-operative scan. It was practically not possible to take the robot to the MRI scanner for in-situ MRI based biopsy procedure. As a result, the script for locating the needle tip location with respect to the target was not developed. However, this should still be used in an eventual SUNRAM 5 based workflow for MRI guided breast biopsy.

The MRI scanner used for the experiment was the Esaote G-scan Brio 0.25T scanner. This is an open bore scanner and of much less strength than that used in a hospital. Therefore, for a fair comparison, the time required to take an actual MRI scan is not included in the evaluation since it is relative to the strength of the MRI scan-

ner and the scanning sequence used. Scanning times can vary from as little as 30 seconds to as high as 15 minutes or more. As mentioned by University of North Carolina School of Medicine (https://www.med.unc.edu/radiology/breastimaging/services/mri-of-the-breast/mri-guided-breast-biopsy/), a standard MRI guided biopsy procedure takes about 60 minutes. Considering the fact that 'most of the time' is required for taking the MRI, an assumption is made that 50% of the time is required for the patient to be taken to the MRI scanner and the actual running of the MRI scan and 50% of the time is required for all the other procedures combined which is 30 minutes. Leaving about 10 minutes aside for all the medical procedures required such as giving the patient an IV drip, inserting a contrast agent, and the post-procedural dressing, time for rest of the procedures comes down to 20 minutes. These 20 minutes involve the time taken to get the patient in and out of the MRI scanner multiple times, by the doctors for locating the lesions and calculating entry point, and for actually performing the biopsy procedure. Performing the actual biopsy procedure again involves tasks such as inserting a stylet through a sheath, creating access to the lesion, marking with an obturator, inserting the biopsy needle, and collecting the samples. For a biopsy procedure with the SUNRAM 5, procedure times have been recorded on the same lines.

No. of sites targeted - 3					
Target No.	Step 1 (min:sec)	Step 2 (min:sec)	Step 3 (min:sec)	Step 4 (min:sec)	Total Procedure Time (min:sec)
1	0:23	0:41	0:22	1:40	3:06
2	0:26	1:20	0:24	1:32	3:42
3	0:30	0:54	0:21	1:41	3:26

Table 5.8: Procedure times recorded for the SUNRAM 5 showing average procedure time around 3 minutes

While operating the workflow, all the applications were already open and available for use. The time required for opening the applications has not been taken into account since it is assumed that in case of an actual MRI guided biopsy, all the required applications would already be open as well. An interpretation of the table is as follows -

- Step 1 - Assuming the pre-operative MRI is already available, this includes the time taken to load the MRI and access it in the 3D slicer app.
- Step 2 - Once the MRI is loaded in the 3D slicer app, this includes the time taken to drop fiducial markers at target locations from MRI and sending these coordinates to MATLAB.
- Step 3 - After the coordinates are available in MATLAB, this includes the time taken to segment the MRI scan to define a coordinate system based on the MRI scan.
- Step 4 - When the MRI scan is segmented and coordinate system defined, this includes the time taken to input the lesion number to be targeted and calculation of the subsequent steps to obtain the robot kinematics. It also includes the time required to operate the robot to the desired location and firing the biopsy gun.

As expected, the timings for Step 2 and Step 4 involve operations that are dependent on operator skill. As a result, there is a larger deviation in the timings. However, on an average, the procedure time evaluated is about 3:25 min. This process involves more or less the same tasks as a normal process based on an MRI guided biopsy. The Stormram 4 required on an average about 1:30 mins to move to a target location Groenhuis (2020). In comparison, the SUNRAM 5 is much faster since as per step 4, entering the lesion number to be targeted, calculating the kinematics and operating the robot to the target along with firing the biopsy gun, everything is

completed on an average in 1:38 mins. In case of the SUNRAM 5, the time required to move the patient multiple times in and out of the MRI scanner is completely gone since the entire procedure can be completed in-situ. Of course, the operation time is greatly dependent on a large number of factors such as operator skills, speed of the computing machine used, and difficulty in locating the lesion. Therefore, this value cannot be considered completely accurate. However, it is a good enough estimate of the time required for the procedure using the SUNRAM 5.

6 Conclusion

The conclusions obtained via the evaluations performed on the SUNRAM 5 are being put forward here. The chapter also discusses the societal impact of this research and its future practical use as a standalone system for undertaking a full clinical MRI based in-situ breast biopsy procedure.

6.1 Conclusion

The SUNRAM 5 is an MR safe robot, 3D printed using rapid prototyping and pneumatically actuated, with a breast fixation system and equipped with a biopsy gun for use in an MRI-guided breast biopsy procedure. The SUNRAM 5 has been implemented with dual-speed stepper motors and theoretically has the potential to improve the positioning accuracy by a maximum 0.1mm in each given direction. By moving at two step sizes simultaneously, the dual-speed stepper motors make the motion of the SUNRAM 5 on an average up to 3.01 times faster than the Stormram 4. Standard measurement procedure by doing a frame by frame analysis of a video was found to be more accurate than a measurement based on a stopwatch since it was devoid of measurement errors of about 0.3 mm. Additionally, the SUNRAM 5 can successfully maintain its frequency of operation at the set frequency. In spite of requiring about 4 times more volume for movement than the Stormram 4, the SUNRAM 5 still has the capability to operate inside a wide bore MRI scanner for in-situ usage. The needle tip accuracy measurements show that the SUNRAM 5 can target the lesions inside a phantom with an average accuracy of 1.24 mm in the X direction and 3.52 mm in the Y direction as per the robot coordinate system. Including the estimated measurement errors, the accuracy of the SUNRAM 5 is identical to the Stormram 4. The breast fixation system of the SUNRAM 5, as opposed to what was expected, causes an increase in average error by about 0.3 mm in both the X and Y direction, most likely due to the sideward deflection in the phantom. The SUNRAM 5, equipped with a biopsy gun, has the ability to take biopsy samples which however are not of the expected quality and further research is required in this area. The development of the easy-to-use user interface app integrated with the possibility to select targets using a mouse click has enabled the SUNRAM to operate in an MRI-guided biopsy workflow with the potential to reduce the actual operation time by about 5-10 minutes per a 60 minute procedure as estimated. In comparison with the Stormram 4, the implementation of the unique breast fixation system along with the use of dual-speed stepper motors, a biopsy gun firing mechanism, and a user interface app has enabled the SUNRAM 5 to be a more complete system ready for an MRI guided breast biopsy procedure while maintaining the targeting accuracy and massive improvement in overall procedure time.

6.2 Societal Impact

The purpose of this research project was the evaluation of the SUNRAM 5 and developing a workflow for the SUNRAM 5 for performing an MRI-guided breast biopsy procedure. However, while searching for the greater good, the value of a research contribution increases with an increase in the societal impact of the research.

Biopsy is the gold standard for histological evaluations. In cases where a lesion is not visible on Ultrasound, an MRI-guided biopsy may be necessary. One of the most crucial things in a biopsy procedure is that the biopsy sample contains at least a part of the lesion in order to avoid additional tissue damage, longer procedure time, and the risk of a false negative outcome. In a standard MRI, the accuracy is highly dependant on the skill of the operator and is also limited by the resolution of the fixation frame grating. Also, as (Radiolo-

gyinfo(https://www.radiologyinfo.org/en/info.cfm?pg=breastbimr)) says, a standard biopsy procedure is also limited by the position of the abnormality in the breast. Smaller lesions are much more difficult to accurately target using the standard procedure. The SUNRAM 5 based biopsy procedure eliminates the need for human skill and can accurately reach target locations which are located at multiples 0.1mm. This is turn greatly reduces the risk of additional tissue damage and a false negative biopsy outcome. This is certainly a positive contribution to patient safety and wellbeing.

The SUNRAM 5 can be used to conduct a biopsy procedure inside an MRI scanner thereby eliminating the need to bring the patient in and out of the MRI scanner multiple times. Keeping this in mind, the procedure based on the SUNRAM 5 has the potential to reduce the overall procedure time by about 5-10 minutes. As per the University of North Carolina School of Medicine (https://www.med.unc.edu/radiology/breastimaging/services/mri-of-the-breast/mri-guided-breast-biopsy/), a standard MRI guided biopsy procedure takes about 60 minutes. This would eventually mean that the SUNRAM 5 based biopsy has the potential to conduct almost 7 MRI guided biopsy procedures in the same time as 6 standard MRI-guided biopsy procedures. This has the potential to reduce waiting times for patients at hospitals. Keeping in mind that multiple operators are required to bring the patient in and out of the MRI scanner, the use of the SUNRAM 5 also has the potential to save man-hours in the hospital environment since fewer operators would be required.

As per the RIVM (https://www.rivm.nl/en/breast-cancer-screening-programme/breast-cancer-in-netherlands), each year about 14000 women in the Netherlands develop invasive breast cancer. Buijs-Van Der Woude et al. (2001) claimed that the average cost per successful biopsy procedure is about 223 Euros including all costs. Additionally, certain fixed costs per year are involved for the upkeep of the equipment and area as well as additional cost is required for the histological evaluation. The SUNRAM 5 reduces the overall procedure time of the biopsy. This directly could affect the biopsy costs with the cost per biopsy reducing for the patients and the number of biopsies conducted in a day increasing leading to shorter waiting times.

6.3 Future Recommendations

The SUNRAM 5 was tested towards working in an MRI-guided breast biopsy workflow. However, a few more further developments are needed before the SUNRAM 5 system can be introduced in actual clinical trials.

- The breast fixation system does not completely perform as expected and an increase in error was observed. It was concluded that the fixation system support from the rear side causes the phantom to deviate in the sideways direction giving increasing errors. Further research is required in order to develop a more complete breast fixation system, something that restricts movement in all directions to have an actual effect.

- The SUNRAM 5 has been implemented with a standard biopsy gun. However, as expected, the quality of the biopsy samples obtained was not as desired. Of course, the stiffness of the breast phantom and the pressure with which the gun is fired plays a role. However, further research is required towards developing an improved design.

- The SUNRAM 5 has a curved base arc in order to enable the needle insertion in a straight direction. However, as per the needle tip reachable workspace evaluation, the targeting area has a major bias towards higher coordinates along the X axis as per the robot coordinate system Figure 4.1. Although repositioning the robot frame is an option, another

option would be to design a straight base rack with capabilities for the needle guide to rotate along the Y axis as per the robot coordinate system Figure 4.1.

- The MATLAB script for the defined MRI coordinate system registration based on the marker positions gives registration errors of about 2mm in the X axis as per the robot coordinate system Figure 4.1. During the development of the script, it was observed that the algorithm, which finds connected components in a geometrically corrected binary scan, does not prove to be efficient enough since it fails to detect the vertical diagonal markers effectively. More research is required in this area to improve registration accuracy.
- The SUNRAM 5 runs in a workflow to complete an MRI-guided breast biopsy procedure. However, the actual operation of the robot is still manual and hence is still dependant on the skill of the operator. Although the SUNRAM 5 is about 3 times faster than the Stormram 4, implementation of automatic movement operation would be a possible solution to eliminate errors due to human operator skill thereby improving movement speed.
- The stepper motors used in the SUNRAM 5 are inherently very accurate and can reach any target that is a multiple of 0.1mm. However, while performing experiments, it was observed many times that the robot takes an extra step on any of the motors presumably due to noise in the controller ADC's or stray pressure in the pneumatic tubes. This extra step can be seen on the controller display. However, with automatic operation, a certain feedback mechanism could be very useful in accurate positioning. Possible options include an optical feedback mechanism or MR safe camera-based feedback system.

Bibliography

[1] Abdelaziz, M., V. Groenhuis, J. Veltman, F. Siepel and S. Stramigioli (2017), Controlling the Stormram 2: An MRI-compatible Robotic System for Breast Biopsy, in *2017 IEEE International Conference on Robotics and Automation (ICRA)*, IEEE, United States, p. 1746, ISBN 978-1-5090-4634-8, doi:10.1109/ICRA.2017.7989206.

[2] Abdelaziz, M. E. M. K. (2016), Designing, implementing and integrating a controller for the MRI compatible robotic breast biopsy system.
http://essay.utwente.nl/71199/

[3] Alterovitz, R., M. Branicky and K. Goldberg (2008), Motion planning under uncertainty for image-guided medical needle steering, **vol. 27**, no.11-12, pp. 1361–1374.

[4] Ball, M. W., A. E. Ross, K. Ghabili, C. Kim, C. Jun, D. Petrisor, L. Pan, J. I. Epstein, K. J. Macura, D. S. Stoianovici et al. (2017), Safety and feasibility of direct magnetic resonance imaging-guided transperineal prostate biopsy using a novel magnetic resonance imaging-safe robotic device, *Urology*, **vol. 109**, pp. 216–221.

[5] Bomers, J., D. Bosboom, G. Tigelaar, J. Sabisch, J. Fütterer and D. Yakar (2017), Feasibility of a 2 nd generation MR-compatible manipulator for transrectal prostate biopsy guidance, **vol. 27**, no.4, pp. 1776–1782.

[6] Van den Bosch, M. R., M. R. Moman, M. Van Vulpen, J. J. Battermann, E. Duiveman, L. J. van Schelven, H. de Leeuw, J. J. Lagendijk and M. A. Moerland (2010), MRI-guided robotic system for transperineal prostate interventions: proof of principle, **vol. 55**, no.5, p. N133.

[7] Buijs-Van Der Woude, T., H. Verkooijen, R. Pijnappel, J. Klinkenbijl, I. B. Rinkes, P. Peeters, E. Buskens, C. study group et al. (2001), Cost comparison between stereotactic large-core-needle biopsy versus surgical excision biopsy in The Netherlands, **vol. 37**, no.14, pp. 1736–1745.

[8] Chan, K. G., T. Fielding and M. Anvari (2016), An image-guided automated robot for MRI breast biopsy, **vol. 12**, no.3, pp. 461–477.

[9] Chinzei, K., N. Hata, F. A. Jolesz and R. Kikinis (2000), MR compatible surgical assist robot: System integration and preliminary feasibility study, in *International Conference on Medical Image Computing and Computer-Assisted Intervention*, Springer, pp. 921–930.

[10] Comber, D. B., D. Cardona, R. Webster III and E. J. Barth (2012), Precision pneumatic robot for MRI-guided neurosurgery, **vol. 6**, no.1, p. 017587.

[11] Cunha, J. A., I.-C. Hsu, J. Pouliot, M. Roach III, K. Shinohara, J. Kurhanewicz, G. Reed and D. Stoianovici (2010), Toward adaptive stereotactic robotic brachytherapy for prostate cancer: demonstration of an adaptive workflow incorporating inverse planning and an MR stealth robot, **vol. 19**, no.4, pp. 189–202.

[12] Franco, E., M. Ristic, M. Rea and W. M. Gedroyc (2016), Robot-assistant for MRI-guided liver ablation: A pilot study, **vol. 43**, no.10, pp. 5347–5356.

[13] Groenhuis, V. (2020), *Robotic systems for breast biopsy using MRI and ultrasound imaging: Optimal guidance to target lesion in deformable tissue*, Ph.D. thesis, University of Twente, Netherlands, doi:10.3990/1.9789036548922.

[14] Groenhuis, V., F. Siepel and S. Stramigioli (2018), Dual-Speed MR Safe Pneumatic Stepper Motors, robotics: Science and Systems 2018, RSS 2018 ; Conference date: 26-06-2018 Through 30-06-2018.
http://roboticsconference.org/

[15] Groenhuis, V., F. Siepel and S. Stramigioli (2019), *Sunram 5: An MR safe robotic system for breast biopsy, driven by pneumatic stepper motors.*

[16] Groenhuis, V., F. Siepel and S. Stramigioli (2020), Miniaturization of MR Safe Pneumatic Rotational Stepper Motors, doi:10.1109/IROS40897.2019.8968262, 2019 IEEE/RSJ International Conference on Intelligent Robots and Systems, IROS 2019 ; Conference date: 04-11-2019 Through 08-11-2019.
https://www.iros2019.org/

[17] Groenhuis, V., F. Siepel, J. Veltman and S. Stramigioli (2017), Design and characterization of Stormram 4: an MRI-compatible robotic system for breast biopsy, in *2017 IEEE/RSJ International Conference on Intelligent Robots and Systems (IROS)*, IEEE, United States, pp. 928–933, ISBN 978-1-5386-2683-2, doi:10.1109/IROS.2017.8202256.

[18] Groenhuis, V., F. Siepel, J. Veltman, J. van Zandwijk and S. Stramigioli (2018), Stormram 4: An MR Safe Robotic System for Breast Biopsy, **vol. 46**, no.10, pp. 1686–1696, ISSN 0090-6964, doi:10.1007/s10439-018-2051-5, springer deal.

[19] Groenhuis, V., F. Siepel, M. Welleweerd, J. Veltman and S. Stramigioli (2018), Sunram 5: An MR Safe Robotic System for Breast Biopsy, pp. 82–83, hamlyn Symposium on Medical Robotics : Pioneering the next generation of medical robotics, HSMR 2018 ; Conference date: 24-06-2018 Through 27-06-2018.
http://hamlyn-robotics.org

[20] Groenhuis, V. and S. Stramigioli (2018), Rapid Prototyping High-Performance MR Safe Pneumatic Stepper Motors, **vol. 23**, no.4, pp. 1843–1853, ISSN 1083-4435, doi:10.1109/TMECH.2018.2840682, early access The supplementary ZIP file with T-63 files was also peer-reviewed. Moved the supplementary ZIP file to the "electronic version" section to make it visible.

[21] Groenhuis, V., E. Tagliabue, M. K. Welleweerd, F. J. Siepel, J. D. Munoz Osorio, B. M. Maris, D. Dall'Alba, U. Zimmermann, P. Fiorini and S. Stramigioli (2020), Deformation Compensation in Robotically-Assisted Breast Biopsy.

[22] Groenhuis, V., J. Veltman, F. Siepel and S. Stramigioli (2017), Stormram 3: A Magnetic Resonance Imaging-Compatible Robotic System for Breast Biopsy, **vol. 24**, no.2, pp. 34–41, ISSN 1070-9932, doi:10.1109/MRA.2017.2680541, special Issue on Surgical Robot Challenge.

[23] Groenhuis, V., J. Veltman and S. Stramigioli (2016), Stormram 2: A MRI-compatible robotic system for breast biopsy, in *Proceedings of The Hamlyn Symposium on Medical Robotics*, Imperial College, pp. 52–53, ISBN 978-0-9563776-7-8.

[24] Guo, Z., Z. Dong, K.-H. Lee, C. L. Cheung, H.-C. Fu, J. D. Ho, H. He, W.-S. Poon, D. T.-M. Chan and K.-W. Kwok (2018), Compact design of a hydraulic driving robot for intraoperative mri-guided bilateral stereotactic neurosurgery, **vol. 3**, no.3, pp. 2515–2522.

[25] Jemal, A., F. Bray, M. M. Center, J. Ferlay, E. Ward and D. Forman (2011), Global cancer statistics, **vol. 61**, no.2, pp. 69–90.

[26] Lang, M. J., A. D. Greer and G. R. Sutherland (2011), Intra-operative robotics: NeuroArm, in *Intraoperative Imaging*, Springer, pp. 231–236.

[27] Masamune, K., L. Ji, M. Suzuki, T. Dohi, H. Iseki and K. Takakura (1998), A newly developed stereotactic robot with detachable drive for neurosurgery, in *International Conference on Medical Image Computing and Computer-Assisted Intervention*, Springer, pp. 215–222.

[28] Monfaredi, R., K. Cleary and K. Sharma (2018), MRI robots for needle-based interventions: systems and technology, **vol. 46**, no.10, pp. 1479–1497.

[29] Moreira, P., G. van de Steeg, T. Krabben, J. Zandman, E. E. Hekman, F. van der Heijden, R. Borra and S. Misra (2017), The miriam robot: A novel robotic system for mr-guided needle insertion in the prostate, **vol. 2**, no.04, p. 1750006.

[30] Navarro-Alarcon, D., S. Singh, T. Zhang, H. L. Chung, K. W. Ng, M. K. Chow and Y. Liu (2017), Developing a compact robotic needle driver for MRI-guided breast biopsy in tight environments, **vol. 2**, no.3, pp. 1648–1655.

[31] Park, S. B., J.-G. Kim, K.-W. Lim, C.-H. Yoon, D.-J. Kim, H.-S. Kang and Y.-H. Jo (2017), A magnetic resonance image-guided breast needle intervention robot system: overview and design considerations, **vol. 12**, no.8, pp. 1319–1331.

[32] de Rooij, M., S. Crienen, J. A. Witjes, J. O. Barentsz, M. M. Rovers and J. P. Grutters (2014), Cost-effectiveness of magnetic resonance (MR) imaging and MR-guided targeted biopsy versus systematic transrectal ultrasound–guided biopsy in diagnosing prostate cancer: a modelling study from a health care perspective, **vol. 66**, no.3, pp. 430–436.

[33] Sergieva, S. (2015), Clinical Application of SPECT-CT in Breast Cancer:, *Archives in Cancer Research*, **vol. 3**, doi:10.21767/2254-6081.100040.

[34] Stoianovici, D., C. Kim, G. Srimathveeravalli, P. Sebrecht, D. Petrisor, J. Coleman, S. B. Solomon and H. Hricak (2013), MRI-safe robot for endorectal prostate biopsy, **vol. 19**, no.4, pp. 1289–1299.

[35] Su, H., M. Zervas, G. A. Cole, C. Furlong and G. S. Fischer (2011), Real-time MRI-guided needle placement robot with integrated fiber optic force sensing, in *2011 IEEE International Conference on Robotics and Automation*, IEEE, pp. 1583–1588.

[36] Vaillant, M., C. Davatzikos, R. H. Taylor and R. N. Bryan (1997), A path-planning algorithm for image-guided neurosurgery, in *CVRMed-MRCAS'97*, Springer, pp. 467–476.

[37] Van Der Maas, P. J., H. J. De Koning, B. M. Van Ineveld, G. J. Van Oortmarssen, J. D. F. Habbema, K. T. N. Lubbe, A. T. Geerts, H. J. Collette, A. L. Verbeek, J. H. Hendriks et al. (1989), The cost-effectiveness of breast cancer screening, **vol. 43**, no.6, pp. 1055–1060.

[38] Varma, T., P. Eldridge, A. Forster, S. Fox, N. Fletcher, M. Steiger, P. Littlechild, P. Byrne, A. Sinnott, K. Tyler et al. (2003), Use of the NeuroMate stereotactic robot in a frameless mode for movement disorder surgery, **vol. 80**, no.1-4, pp. 132–135.

[39] Yang, B., S. Roys, U.-X. Tan, M. Philip, H. Richard, R. P. Gullapalli and J. P. Desai (2014), Design, development, and evaluation of a master–slave surgical system for breast biopsy under continuous MRI, **vol. 33**, no.4, pp. 616–630.

[40] Zhang, T., D. Navarro-Alarcon, K. W. Ng, M. K. Chow, Y.-h. Liu and H. L. Chung (2016), A novel palm-shape breast deformation robot for MRI-guided biopsy, in *2016 IEEE International Conference on Robotics and Biomimetics (ROBIO)*, IEEE, pp. 527–532.